Impact of quark flavor violating SUSY on $h(125)$ decays at future lepton colliders

Helmut Eberl,[1] Keisho Hidaka,[2] and Elena Ginina[1]

[1]*Institut für Hochenergiephysik der Österreichischen Akademie der Wissenschaften, A-1050 Vienna, Austria*
[2]*Department of Physics, Tokyo Gakugei University, Koganei, Tokyo 184-8501, Japan*

(Received 28 May 2024; accepted 8 October 2025; published 9 January 2026)

We study the *CP*-even neutral Higgs boson decays $h^0 \to c\bar{c}, b\bar{b}, b\bar{s}, \gamma\gamma, gg$ in the minimal supersymmetric standard model (MSSM) with a general quark flavor violation (QFV) due to squark generation mixings, identifying the h^0 as the Higgs boson with a mass of 125 GeV. We compute the widths of the h^0 decays to $c\bar{c}, b\bar{b}, b\bar{s}$ at the full one-loop level. For the h^0 decays to $\gamma\gamma$ and gg, we compute the widths at NLO QCD level. *For the first time*, we perform a systematic MSSM parameter scan for these widths, respecting all the relevant theoretical and experimental constraints, such as those from B-meson data, and the 125 GeV Higgs boson data from recent LHC experiments, as well as the limits on supersymmetric (SUSY) particle (sparticle) masses from the LHC experiments. We also take into account the expected sparticle mass limits from the future HL-LHC experiment in our analysis. *In strong contrast to* the usual studies in the MSSM with minimal flavor violation (MFV), we find that the deviations of these MSSM decay widths from the Standard Model (SM) values can be quite sizable and that there are significant correlations among these deviations. All of these sizable deviations in the h^0 decays are mainly due to large scharm-stop mixing and large sstrange-sbottom mixing. Such sizable deviations from the SM can be observed at high signal significance in future lepton colliders such as ILC, CLIC, CEPC, FCC-ee, and muon collider *even after* the failure of SUSY particle discovery at the HL-LHC. In case the deviation pattern shown here is really observed at the lepton colliders, then it would strongly suggest the discovery of QFV SUSY (the MSSM with general QFV).

DOI: 10.1103/8tsj-8tpc

I. INTRODUCTION

What is the Standard Model (SM)-like Higgs boson with mass of 125 GeV discovered at LHC [1,2]? It can be the Higgs boson of the SM. It can be a Higgs boson of a new physics (NP) theory beyond the SM. This is one of the most important issues in the field of present particle physics. The detailed study of the properties (such as mass and couplings) of the SM-like Higgs boson could shed light on this issue and the way to the NP theory [3]. Here, we study a possibility that the discovered SM-like Higgs boson is the lighter *CP* even neutral Higgs boson h^0 of the minimal supersymmetric standard model (MSSM), focusing on the decays $h^0 \to c\bar{c}, b\bar{b}, b\bar{s}, \gamma\gamma, gg$, where c, b, s, γ, and g are c-, b-, s-quarks, photon, and gluon, respectively. In order to investigate such a possibility, we compute the widths of these decays in the MSSM with general quark-flavor violation (QFV) due to squark generation mixing according to our previous works [4–6] and study the deviations of the MSSM widths from the SM widths.

The deviations of the SM-like Higgs boson decay widths from their SM values are usually estimated to be rather small (typically several percent level or less) in the MSSM with minimal flavor violation (MFV), where the only source of quark-flavor violation is the Cabibbo-Kobayashi-Maskawa (CKM) quark-mixing matrix [7–12]. In the present article, however, we show that the situation changes drastically yielding significant enhancement of the deviations in the widths once we switch-on the general QFV in the MSSM, by performing a systematic MSSM parameter scan respecting all the relevant theoretical and experimental constraints.[1]

In [14–19], it was shown that the general QFV in the MSSM can also enhance QFV decays $h^0 \to b\bar{s}$ and $h^0 \to \bar{b}s$. These analyses are rather old. In the present paper, we update them, especially by taking into account the expected mass limits for the superpartner particles and

Published by the American Physical Society under the terms of the Creative Commons Attribution 4.0 International license. Further distribution of this work must maintain attribution to the author(s) and the published article's title, journal citation, and DOI. Funded by SCOAP³.

[1]The decay $h^0 \to c\bar{c}$ was not studied in [7–12]. The decays $h^0 \to c\bar{c}, \gamma\gamma, gg$ in the MSSM with QFV were studied in [13]. However, the important QFV parameters M^2_{Q23}, M^2_{U23}, and M^2_{D23} (which are defined in Sec. II) were neglected and the systematic MSSM parameter scan respecting all the relevant theoretical and experimental constraints was not performed in [13].

the heavier MSSM Higgs bosons H^0, A^0, H^+ from the future HL-LHC experiment.

On the experimental side, the widths of these decays, $h^0 \to c\bar{c}, b\bar{b}, \gamma\gamma, gg$ (or corresponding effective couplings) can be measured precisely and *model independently* at future lepton colliders, such as ILC, CLIC, CEPC, FCC-ee, and muon-collider (MuC) [20,21].[2] This enables us to clarify the possibility that the discovered SM-like Higgs boson is the lighter CP even neutral Higgs boson h^0 of the MSSM.

In Sec. II, we introduce the supersymmetric (SUSY) QFV parameters originating from the squark mass matrices. Details of our parameter scan are given in Sec. III. In Sec. IV, we study the deviations of the MSSM widths from the SM widths for the decays $h^0 \to c\bar{c}, b\bar{b}, b\bar{s}, \gamma\gamma, gg$ and analyze their behavior in the MSSM with general QFV. The summary and conclusion are in Sec. V. All relevant constraints are listed in Appendix A, and the expected errors in the deviation measurements at future lepton colliders are listed in Appendix B. ILC sensitivity to the branching ratio $B(h^0 \to bs)$ is discussed in Appendix C, and consistency of the MSSM predictions for coupling modifiers with the LHC data is discussed in Appendix D.

II. SQUARK MASS MATRICES IN THE MSSM WITH GENERAL QFV

In the super-CKM basis of $\tilde{q}_{0\gamma} = (\tilde{q}_{1L}, \tilde{q}_{2L}, \tilde{q}_{3L}, \tilde{q}_{1R}, \tilde{q}_{2R}, \tilde{q}_{3R}), \gamma = 1, \ldots 6$, with $(q_1, q_2, q_3) = (u, c, t)$, (d, s, b), the up-type and down-type squark mass squared matrices $\mathcal{M}^2_{\tilde{q}}, \tilde{q} = \tilde{u}, \tilde{d}$, at the SUSY scale have the following most general 3×3 block form [23]:

$$\mathcal{M}^2_{\tilde{q}} = \begin{pmatrix} \mathcal{M}^2_{\tilde{q},LL} & \mathcal{M}^2_{\tilde{q},LR} \\ \mathcal{M}^2_{\tilde{q},RL} & \mathcal{M}^2_{\tilde{q},RR} \end{pmatrix}, \qquad \tilde{q} = \tilde{u}, \tilde{d}. \tag{1}$$

Nonzero off diagonal terms of the 3×3 blocks $\mathcal{M}^2_{\tilde{q},LL}$, $\mathcal{M}^2_{\tilde{q},RR}$, $\mathcal{M}^2_{\tilde{q},LR}$, and $\mathcal{M}^2_{\tilde{q},RL}$ explicitly violate quark flavor in the squark sector of the MSSM. The left-left and right-right blocks in Eq. (1) are given by

$$\begin{aligned} \mathcal{M}^2_{\tilde{u}(\tilde{d}),LL} &= M^2_{Q_{u(d)}} + D_{\tilde{u}(\tilde{d}),LL}\mathbf{1} + \hat{m}^2_{u(d)}, \\ \mathcal{M}^2_{\tilde{u}(\tilde{d}),RR} &= M^2_{U(D)} + D_{\tilde{u}(\tilde{d}),RR}\mathbf{1} + \hat{m}^2_{u(d)}, \end{aligned} \tag{2}$$

where $M^2_{Q_u} = V_{\mathrm{CKM}} M^2_Q V^\dagger_{\mathrm{CKM}}$, $M^2_{Q_d} \equiv M^2_Q$, $M^2_{Q,U,D}$ are the Hermitian soft SUSY-breaking mass squared matrices of the squarks, $D_{\tilde{u}(\tilde{d}),LL}$, $D_{\tilde{u}(\tilde{d}),RR}$ are the D terms, and $\hat{m}_{u(d)}$ are the diagonal mass matrices of the up(down)-type quarks. $M^2_{Q_u}$ is related with $M^2_{Q_d}$ by the CKM matrix V_{CKM} due to the $SU(2)_{\mathrm{L}}$ symmetry. The left-right and right-left blocks of Eq. (1) are given by

$$\mathcal{M}^2_{\tilde{u}(\tilde{d}),RL} = \mathcal{M}^{2\dagger}_{\tilde{u}(\tilde{d}),LR} = \frac{v_2(v_1)}{\sqrt{2}} T_{U(D)} - \mu^* \hat{m}_{u(d)} \cot\beta(\tan\beta), \tag{3}$$

where $T_{U,D}$ are the soft SUSY-breaking trilinear coupling matrices of the up-type and down-type squarks entering the Lagrangian $\mathcal{L}_{\mathrm{int}} \supset -(T_{U\alpha\beta}\tilde{u}^\dagger_{\alpha R}\tilde{u}_{\beta L}H^0_2 + T_{D\alpha\beta}\tilde{d}^\dagger_{\alpha R}\tilde{d}_{\beta L}H^0_1)$, μ is the Higgsino mass parameter, and $\tan\beta = v_2/v_1$ with $v_{1,2} = \sqrt{2}\langle H^0_{1,2}\rangle$. The squark mass squared matrices are diagonalized by the 6×6 unitary matrices $U^{\tilde{q}}$, $\tilde{q} = \tilde{u}, \tilde{d}$, such that

$$U^{\tilde{q}} \mathcal{M}^2_{\tilde{q}} (U^{\tilde{q}})^\dagger = \mathrm{diag}(m^2_{\tilde{q}_1}, \ldots, m^2_{\tilde{q}_6}), \tag{4}$$

with $m_{\tilde{q}_1} < \ldots < m_{\tilde{q}_6}$. The physical mass eigenstates $\tilde{q}_i, i = 1, \ldots, 6$ are given by $\tilde{q}_i = U^{\tilde{q}}_{i\alpha}\tilde{q}_{0\alpha}$.

In this paper, we focus on the $\tilde{c}_L - \tilde{t}_L$, $\tilde{c}_R - \tilde{t}_R$, $\tilde{c}_R - \tilde{t}_L$, $\tilde{c}_L - \tilde{t}_R$, $\tilde{s}_L - \tilde{b}_L$, $\tilde{s}_R - \tilde{b}_R$, $\tilde{s}_R - \tilde{b}_L$, and $\tilde{s}_L - \tilde{b}_R$ mixing, which is described by the QFV parameters $M^2_{Q_u 23} \simeq M^2_{Q23}$, M^2_{U23}, T_{U23}, T_{U32}, M^2_{Q23}, M^2_{D23}, T_{D23}, and T_{D32}, respectively. We will also often refer to the quark-flavor conserving (QFC) parameters T_{U33} and T_{D33}, which induce the $\tilde{t}_L - \tilde{t}_R$ and $\tilde{b}_L - \tilde{b}_R$ mixing, respectively, and play an important role in this study.

The slepton parameters are defined analogously to the squark ones. In our analysis, we assume that there is no SUSY lepton-flavor violation. We also assume that R parity is conserved and that the lightest neutralino $\tilde{\chi}^0_1$ is the lightest SUSY particle (LSP). All the parameters in this study are assumed to be real, except the CKM matrix V_{CKM}.

III. PARAMETER SCAN

In our MSSM parameter scan, we take into account all the relevant constraints, i.e., theoretical constraints from vacuum stability conditions and experimental constraints, such as those from K- and B-meson data, electroweak precision data, and the H^0 mass and coupling data from recent LHC experiments, as well as the SUSY particle (sparticle) mass limits from current LHC experiments (see Appendix A). Here, H^0 is the discovered SM-like Higgs boson, which we identify as the lightest CP even neutral Higgs boson h^0 in the MSSM. Concerning squark generation mixings, we only consider the mixing between the second and third generation of squarks. The mixing between the first and the second generation squarks is strongly constrained by the K- and D-meson data [24,25]. The experimental constraints on the mixing of the first and third generation squarks are not so strong [26], but we do not consider this mixing since its effect is essentially similar to that of the mixing of the second and third

[2]The effective couplings of $g(h^0 b\bar{b})$, $g(h^0\gamma\gamma)$ and $g(h^0 gg)$ can be measured rather precisely but *model dependently* by a global fit at HL-LHC [20–22]. Moreover, it is difficult to measure the coupling $g(h^0 c\bar{c})$ at LHC and HL-LHC due to the difficulty of the c-tagging and the huge hadronic QCD background [22].

TABLE I. Scanned ranges and fixed values of the MSSM parameters (in units of GeV or GeV^2, except for $\tan\beta$). The parameters that are not shown explicitly are taken to be zero. $M_{1,2,3}$ are the U(1), SU(2), SU(3) gaugino mass parameters.

$\tan\beta$	M_1	M_2	M_3	μ	m_{A^0}(pole)
10/80	100/2500	100/2500	2500/5000	100/2500	1350/6000

M^2_{Q22}	M^2_{Q33}	$\lvert M^2_{Q23}\rvert$	M^2_{U22}	M^2_{U33}	$\lvert M^2_{U23}\rvert$
$2500^2/4000^2$	$2500^2/4000^2$	$<1000^2$	$1000^2/4000^2$	$600^2/3000^2$	$<2000^2$

M^2_{D22}	M^2_{D33}	$\lvert M^2_{D23}\rvert$	$\lvert T_{U23}\rvert$	$\lvert T_{U32}\rvert$	$\lvert T_{U33}\rvert$
$2500^2/4000^2$	$1000^2/3000^2$	$<2000^2$	<4000	<4000	<5000

$\lvert T_{D23}\rvert$	$\lvert T_{D32}\rvert$	$\lvert T_{D33}\rvert$	$\lvert T_{E33}\rvert$
<3000	<3000	<4000	<500

M^2_{Q11}	M^2_{U11}	M^2_{D11}	M^2_{L11}	M^2_{L22}	M^2_{L33}	M^2_{E11}	M^2_{E22}	M^2_{E33}
4500^2	4500^2	4500^2	1500^2	1500^2	1500^2	1500^2	1500^2	1500^2

generation squarks. We generate the input parameter points by using random numbers in the ranges shown in Table I, where some parameters are fixed as given in the last box. All input parameters are $\overline{\rm DR}$ parameters defined at scale $Q = 1$ TeV, except m_{A^0}(pole) which is the pole mass of the CP odd Higgs boson A^0. The parameters that are not shown explicitly are taken to be zero. The entire scan range lies in the decoupling Higgs limit, i.e., in the scenarios with large $\tan\beta \geq 10$ and large $m_{A^0} \geq 1350$ GeV (see Table I), respecting the fact that the discovered Higgs boson is SM-like. It is well known that the lightest MSSM Higgs boson h^0 is SM-like (including its couplings) in this limit. We do not assume the GUT relation for the gaugino masses M_1, M_2, M_3. The masses and mixing matrices of the SUSY particles and the Higgs bosons are renormalized basically at one-loop level by using the public code SPheno-v3.3.8 [27,28][3] based on the technique given in [30]. From 377180 input points generated in the scan, 3208 points survived all constraints. These are 0.85% of the generated points. We show these survival points in all scatter plots in this article.

IV. 125 GeV HIGGS BOSON DECAYS IN THE MSSM WITH GENERAL QFV

We compute the decay widths $\Gamma(h^0 \to c\bar{c})$, $\Gamma(h^0 \to b\bar{b})$, and $\Gamma(h^0 \to b\bar{s}/\bar{b}s)$ at full 1-loop level in the $\overline{DR}$ renormalization scheme in the MSSM with general QFV [4,5] and study the deviation of the MSSM predictions from the SM ones. We also compute the decay widths $\Gamma(h^0 \to gg)$ and $\Gamma(h^0 \to \gamma\gamma)$ at the next-to-leading order (NLO) QCD level in the $\overline{DR}$ renormalization scheme in the MSSM with general QFV [6] and study the deviation of the MSSM widths from the SM ones, where g is a gluon and γ is a photon. As the h^0 decays to gg and $\gamma\gamma$ are loop-induced decays, these decays are sensitive to new physics.

Here, we remark the differences between our previous works [4–6] and the present work: In the present work, we update the constraints on the MSSM parameters significantly including the expected sparticle mass limits from the future HL-LHC experiments, and study also the branching ratio of the explicitly QFV decay $B(h^0 \to b\bar{s}/\bar{b}s)$ and the correlations among the deviations of the MSSM widths of the various decay modes from the corresponding SM ones.

A. Expectations

We find that large squark trilinear couplings $T_{U23,32,33}$, $T_{D23,32,33}$, large M^2_{Q23}, M^2_{U23}, M^2_{D23}, large bottom Yukawa coupling Y_b for large $\tan\beta$, and large top Yukawa coupling Y_t can lead to large MSSM 1-loop contributions to these decay widths, resulting in sizable deviation of the MSSM widths from the SM values. This is mainly due to the following reasons:

The lighter up-type squarks $\tilde{u}_{1,2,3}$ are strong $\tilde{c}_{L,R}$-$\tilde{t}_{L,R}$ mixtures for large M^2_{Q23}, M^2_{U23}, $T_{U23,32,33}$. The lighter down-type squarks $\tilde{d}_{1,2,3}$ are strong $\tilde{s}_{L,R}$-$\tilde{b}_{L,R}$ mixtures for large M^2_{Q23}, M^2_{D23}, $T_{D23,32,33}$. Here, note that $|T_{U23,32,33}|$ the size of which are controlled by Y_t due to the vacuum stability conditions can be large because of large Y_t and that

[3]This version SPheno-v3.3.8 implements full flavor (generation) mixings in the sfermion (squarks and sleptons) sector as described in Sec. II and calculates the masses and mixings of the SUSY particles and the MSSM Higgs bosons $h^0, H^0, A^0, H^\pm$ taking into accounts the full flavor mixings in the sfermion sector [29].

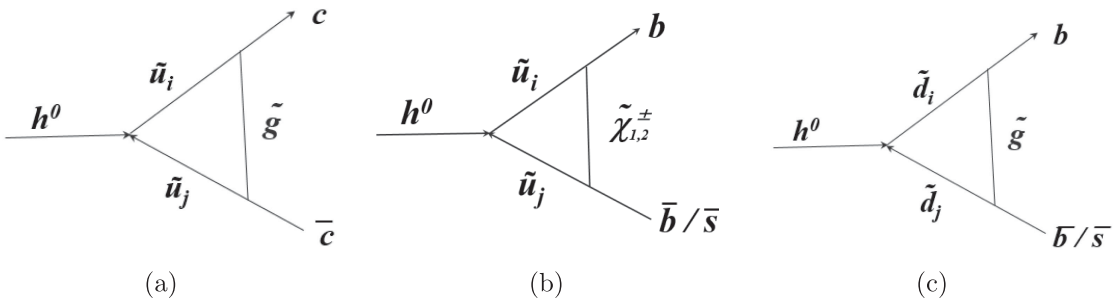

FIG. 1. (a) The $\tilde{u}_i - \tilde{g}$ loop corrections to $\Gamma(h^0 \to c\bar{c})$, (b) the $\tilde{u}_i - \tilde{\chi}^{\pm}_{1,2}$ loop, and (c) the $\tilde{d}_i - \tilde{g}$ loop corrections to $\Gamma(h^0 \to b\bar{b}/\bar{s})$.

$|T_{D23,32,33}|$ the size of which are controlled by Y_b due to the vacuum stability conditions can be large thanks to large Y_b for large $\tan\beta$ [see Eqs. (A1)–(A4) in Appendix A]. In the following, we assume these setups.

1. Expectations for fermionic decays

The main MSSM 1-loop corrections to $\Gamma(h^0 \to c\bar{c})$ stem from the lighter up-type squarks ($\tilde{u}_{1,2,3}$)-gluino ($\tilde{g}$) loops at the decay vertex, which have $h^0 - \tilde{u}_i - \tilde{u}_j$ couplings containing $H^0_2 - \tilde{c}_R - \tilde{t}_L$, $H^0_2 - \tilde{c}_L - \tilde{t}_R$, $H^0_2 - \tilde{t}_L - \tilde{t}_R$ couplings, i.e., $T_{U23,32,33}$ [see Fig. 1(a)]. Note that h^0 is a mixture of $\mathrm{Re}(H^0_1)$ (which couples to the down-type squarks $\tilde{d}_i$) and $\mathrm{Re}(H^0_2)$ (which couples to the up-type squarks $\tilde{u}_i$), i.e., $h^0 = -\sin\alpha(\sqrt{2}\mathrm{Re}(H^0_1) - v_1) + \cos\alpha(\sqrt{2}\mathrm{Re}(H^0_2) - v_2)$ and that h^0 is dominated by $\mathrm{Re}(H^0_2)$ component in our decoupling Higgs scenario with large $m_{A^0}(>1350$ GeV) and large $\tan\beta(>10)$ (see Table I). Hence, the large $\mathrm{Re}(H^0_2)$ component of h^0 and the large trilinear couplings $T_{U23,32,33}$ can enhance the $h^0 - \tilde{u}_i - \tilde{u}_j$ couplings, which together with the large QCD couplings involved can result in a strong enhancement of the $\tilde{u}_i$-$\tilde{g}$ loop corrections to $\Gamma(h^0 \to c\bar{c})$, leading to a large deviation of the MSSM width $\Gamma(h^0 \to c\bar{c})$ from its SM value.

Here, note that $\tilde{u}_i$-neutralino ($\tilde{\chi}^0_i$) loops and $\tilde{d}_i$-chargino ($\tilde{\chi}^{\pm}_{1,2}$) loops at the decay vertex are not so important by the following reason with $\tilde{\chi}^0_i$ and $\tilde{\chi}^{\pm}_{1,2}$ being mixtures of photino $\tilde{\gamma}$, zino $\tilde{Z}$, and neutral Higgsinos $\tilde{H}^0_{1,2}$ and mixtures of charged wino $\tilde{W}^{\pm}$ and charged higgsino $\tilde{H}^{\pm}$, respectively: (i) The former loops, where h^0 directly couples to $\tilde{u}_i - \tilde{u}_j$, are suppressed by the relatively small electroweak-Yukawa couplings of the neutralino to c and $\tilde{u}_i$ compared with the QCD couplings of gluino to c and $\tilde{u}_i$ in the $\tilde{u}_i - \tilde{g}$ loops. (ii) The former loops, where h^0 directly couples to the neutralino, are also suppressed by the relatively small couplings of the neutralino and cannot be enhanced by the large trilinear couplings $T_{U23,32,33}$. (iii) The latter loops, where h^0 directly couples to $\tilde{d}_i - \tilde{d}_j$, are suppressed by the small $\mathrm{Re}(H^0_1)$ component of h^0 though they can be enhanced by the large trilinear couplings $T_{D23,32,33}$. They are further suppressed by the relatively small electroweak-Yukawa couplings of the chargino to c and $\tilde{d}_i$ compared with the QCD couplings. (iv) The latter loops where h^0 directly couples to the chargino are also suppressed by the relatively small electroweak-Yukawa couplings of the chargino to c and $\tilde{d}_i$ and cannot be enhanced by the large trilinear couplings $T_{D23,32,33}$.

The main MSSM 1-loop corrections to $\Gamma(h^0 \to b\bar{b})$ and $\Gamma(h^0 \to b\bar{s}/\bar{b}s)$ stem from (i) $\tilde{u}_{1,2,3}$-chargino ($\tilde{\chi}^{\pm}_{1,2}$) loops at the decay vertex which have $h^0 - \tilde{u}_i - \tilde{u}_j$ couplings to be enhanced by large $T_{U23,32,33}$ [see Fig. 1(b)][4] and (ii) $\tilde{d}_{1,2,3}$-$\tilde{g}$ loops at the decay vertex which have $h^0 - \tilde{d}_i - \tilde{d}_j$ couplings containing $H^0_1 - \tilde{s}_R - \tilde{b}_L$, $H^0_1 - \tilde{s}_L - \tilde{b}_R$, $H^0_1 - \tilde{b}_L - \tilde{b}_R$ couplings, i. e., $T_{D23,32,33}$ [see Fig. 1(c)].[5] Hence, large trilinear couplings $T_{U23,32,33}$ and $T_{D23,32,33}$ can enhance the MSSM 1-loop corrections to $\Gamma(h^0 \to b\bar{b})$ and $\Gamma(h^0 \to b\bar{s}/\bar{b}s)$ due to the $\tilde{u}_i$-$\tilde{\chi}^{\pm}_{1,2}$ and $\tilde{d}_i$-$\tilde{g}$ loops, leading to a large deviation of the MSSM widths $\Gamma(h^0 \to b\bar{b})$ and $\Gamma(h^0 \to b\bar{s}/\bar{b}s)$ from their SM values.

Note that the wave function corrections for the external h^0 in the decays $h^0 \to c\bar{c}/b\bar{b}$ which have the $h^0 - \tilde{u}_i - \tilde{u}_j$ and $h^0 - \tilde{d}_i - \tilde{d}_j$ couplings (for $\tilde{u}_i$ and $\tilde{d}_i$ loops, respectively) can also be enhanced by the large trilinear couplings $T_{U23,32,33}$ and $T_{D23,32,33}$, resulting in a further enhancement of the MSSM 1-loop corrections to the widths $\Gamma(h^0 \to c\bar{c}/b\bar{b})$.

Here, we remark that the MSSM one-loop corrections to the decay amplitude for $h^0 \to c\bar{c}$ are expected to be significantly larger than those for $h^0 \to b\bar{b}$ due to the following reasons:

(i) The main MSSM 1-loop corrections to $h^0 \to c\bar{c}$ stem from $\tilde{u}_i$-$\tilde{g}$ loops [Fig. 1(a)]. The main MSSM 1-loop corrections to $h^0 \to b\bar{b}$ stem from $\tilde{u}_i$-$\tilde{\chi}^{\pm}_j$ loops [Fig. 1(b)] and $\tilde{d}_i$-$\tilde{g}$ loops [Fig. 1(c)].

[4]Note that the $\tilde{u}_{1,2,3}$-$\tilde{\chi}^{\pm}_{1,2}$ loops, where h^0 couples directly to $\tilde{\chi}^{\pm}_{1,2}$, cannot be enhanced by the large $T_{U23,32,33}$, and hence, they are not so important.

[5]Here, note that the $h^0 - \tilde{d}_i - \tilde{d}_j$ couplings are suppressed by the small $\mathrm{Re}(H^0_1)$ component of h^0 but can be enhanced by large $T_{D23,32,33}$. Note also that $\tilde{d}_{1,2,3}$-$\tilde{\chi}^0_i$ loops at the decay vertex are not so important compared with $\tilde{d}_{1,2,3}$-$\tilde{g}$ loops at the vertex by a reason similar to the reason why the $\tilde{u}_i$-$\tilde{\chi}^0_i$ loop corrections to $\Gamma(h^0 \to c\bar{c})$ are suppressed compared with the $\tilde{u}_i$-$\tilde{g}$ loop corrections.

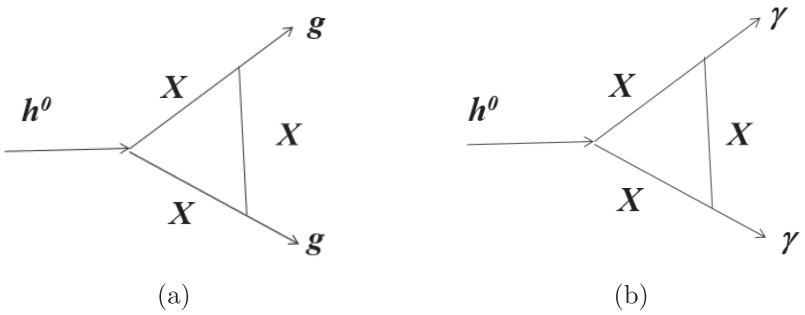

FIG. 2. (a) The SM (X = top quark) and MSSM (X = $\tilde{u}_{1,2,3}$) loop contributions to $\Gamma(h^0 \to gg)$, and (b) the SM (X = W^+ boson, top quark) and MSSM (X = $\tilde{u}_{1,2,3}$) loop contributions to $\Gamma(h^0 \to \gamma\gamma)$. The NLO QCD correction diagrams are not shown in these figures. For (a) $h^0 \to gg$, the MSSM ($\tilde{u}_i$) loop diagrams with the contact interactions of $\tilde{u}_i$-$\tilde{u}_i$-gluon-gluon are not shown. For (b) $h^0 \to \gamma\gamma$, the SM (W^+) loop diagram with that of W-W-γ-γ and the MSSM ($\tilde{u}_i$) loop diagrams with those of $\tilde{u}_i$-$\tilde{u}_i$-γ-γ are not shown.

(ii) The $\tilde{u}_i$-$\tilde{\chi}_j^{\pm}$ loops of Fig. 1(b) are suppressed by the relatively small electroweak-Yukawa couplings of $\tilde{\chi}_j^{\pm}$ compared with the $\tilde{u}_i$-$\tilde{g}$ loops of Fig. 1(a) having the large QCD couplings of $\tilde{g}$.

(iii) The $\tilde{d}_i$-$\tilde{g}$ loops of Fig. 1(c) are suppressed by the relatively small $h^0 - \tilde{d}_i - \tilde{d}_j$ couplings due to the small $\mathrm{Re}(H_1^0)$ component of h^0 compared with the $\tilde{u}_i$-$\tilde{g}$ loops of Fig. 1(a).

(iv) Hence, the MSSM one-loop corrections to the decay amplitude for $h^0 \to c\bar{c}$ [Fig. 1(a)] are expected to be significantly larger than those for $h^0 \to b\bar{b}$ [Figs. 1(b) and 1(c)].

On the other hand, the SM width $\Gamma(h^0 \to c\bar{c})_{\mathrm{SM}}$ is much smaller than $\Gamma(h^0 \to b\bar{b})_{\mathrm{SM}}$ mainly due to the much smaller charm Yukawa coupling than the bottom Yukawa one, which together with the item (iv), results in *much larger* relative deviation of the MSSM width from the SM width for the decay $h^0 \to c\bar{c}$ than that for $h^0 \to b\bar{b}$ [see Eq. (5)] *in strong contrast to usual expectations*. We will see this tendency explicitly in the plots shown below (e.g., see Fig. 3).

2. Expectations for bosonic decays

Similar arguments hold for the loop-induced decays $h^0 \to gg, \gamma\gamma$. The main SM 1-loop contribution to $\Gamma(h^0 \to gg)$ stems from the top-quark loop. The bottom-quark loop contribution to this width is much suppressed by the small $\mathrm{Re}(H_1^0)$ component of h^0 in our decoupling Higgs scenario. The main MSSM 1-loop contributions to $\Gamma(h^0 \to gg)$ stem from the lighter up-type squark ($\tilde{u}_{1,2,3}$) loops, which have $h^0 - \tilde{u}_i - \tilde{u}_i$ couplings [see Fig. 2(a)]. The large trilinear couplings $T_{U23,32,33}$ can enhance the $h^0 - \tilde{u}_i - \tilde{u}_i$ couplings and hence, the $\tilde{u}_i$ loops, resulting in sizable deviation of the MSSM width $\Gamma(h^0 \to gg)$ from its SM value. The lighter down-type squark ($\tilde{d}_{1,2,3}$) loop contributions to this width are suppressed by the small $\mathrm{Re}(H_1^0)$ component of h^0.

The main SM 1-loop contributions to $\Gamma(h^0 \to \gamma\gamma)$ stem from W^+ boson and top-quark loops. The bottom-quark and tau-lepton loop contributions to this width are suppressed by the small $\mathrm{Re}(H_1^0)$ component of h^0. The main MSSM 1-loop contributions to $\Gamma(h^0 \to \gamma\gamma)$ stem from the lighter up-type squark ($\tilde{u}_{1,2,3}$) loops, which have $h^0 - \tilde{u}_i - \tilde{u}_i$ couplings [see Fig. 2(b)]. The large trilinear couplings $T_{U23,32,33}$ can enhance the $h^0 - \tilde{u}_i - \tilde{u}_i$ couplings and hence, the $\tilde{u}_i$ loops, leading to a sizable deviation of the MSSM width $\Gamma(h^0 \to \gamma\gamma)$ from its SM value. The lighter down-type squark ($\tilde{d}_{1,2,3}$) and the charged slepton loop contributions to this width are suppressed by the small $\mathrm{Re}(H_1^0)$ component of h^0. The chargino loops can also contribute to this width, but they can not be enhanced by the large trilinear couplings $T_{U23,32,33}$. The H^+ boson loop contribution to this width is strongly suppressed by its large mass m_{H^+} ($\simeq m_{A^0}$) in our decoupling Higgs scenario with large $m_{A^0}(>1350\ \mathrm{GeV})$ and large $\tan\beta(>10)$ (see Table I). Here, note that the deviation of the MSSM width $\Gamma(h^0 \to \gamma\gamma)$ from its SM value is not so large since the W^+ boson loop contribution dominates this width.

B. Scatter plot analysis

We compute the decay widths $\Gamma(h^0 \to X\bar{X})$ ($X = c, b$) and $\Gamma(h^0 \to bs) \equiv \Gamma(h^0 \to b\bar{s}) + \Gamma(h^0 \to \bar{b}s)$ at full 1-loop level in the $\overline{DR}$ renormalization scheme in the MSSM with general QFV using Fortran codes developed by us [4,5].[6] We compute the decay widths $\Gamma(h^0 \to XX)$ ($X = g, \gamma$) at the NLO QCD level in the $\overline{DR}$ renormalization scheme in the MSSM with general QFV using Fortran

[6]The SM widths $\Gamma(h^0 \to X\bar{X})_{\mathrm{SM}}$ ($X = c, b$) are computed in Refs. [31,32], but we do not use these SM widths. Instead, we compute the SM widths $\Gamma(h^0 \to X\bar{X})_{\mathrm{SM}}$ ($X = c, b$) by taking the decoupling SUSY/Higgs limit of the MSSM width $\Gamma(h^0 \to X\bar{X})_{\mathrm{MSSM}}$, i.e., the limit of large SUSY mass scale M_{SUSY}, large m_{A^0}(pole), large $\tan\beta$, and no SUSY QFV (no squark generation mixing) in order to calculate the relative deviation of the MSSM width $\Gamma(h^0 \to X\bar{X})_{\mathrm{MSSM}}$ from the SM width $\Gamma(h^0 \to X\bar{X})_{\mathrm{SM}}$ at full 1-loop level *consistently*. We have obtained $\Gamma(h^0 \to c\bar{c})_{\mathrm{SM}} = 0.128$ MeV and $\Gamma(h^0 \to b\bar{b})_{\mathrm{SM}} = 2.89$ MeV.

codes developed by us [6].[7] The details of the computation of the decay widths $\Gamma(h^0 \to XX)$ $(X = g, \gamma)$ at the NLO QCD level in the MSSM with general QFV are explained in Sec. 3 of [6] (see especially footnote 1 in Sec. 3 of [6]).

In the following, we will show scatter plots in various planes related with these decay widths obtained from the MSSM parameter scan described above (see Table I), respecting all the relevant constraints (see Appendix A).

1. Definition of relative deviations from SM predictions

We define the relative deviation of the decay width $\Gamma(X)(\equiv\Gamma(h^0 \to X\bar{X}))$ from the SM width as follows:

$$\mathrm{DEV(X)} \equiv \frac{\Gamma(\mathrm{X})}{\Gamma(\mathrm{X})_{\mathrm{SM}}} - 1 (X = \mathrm{c, b, g}, \gamma). \tag{5}$$

Here, $\Gamma(X)_{\mathrm{SM}}$ is the SM prediction for the decay width $\Gamma(X)$.

According to Ref. [21], we define the effective h^0XX coupling $g(h^0XX)$ as follows:

$$g(h^0XX)^2 \equiv \frac{\Gamma(\mathrm{X})}{\Gamma(\mathrm{X})_{\mathrm{SM}}}. \tag{6}$$

As the SM effective coupling $g(h^0XX)_{\mathrm{SM}} = 1$ by definition, the so-called coupling modifier $\kappa_X(\equiv g(h^0XX)/g(h^0XX)_{\mathrm{SM}})$ is equal to $g(h^0XX)$. The relative deviation DEV(X) is related with the effective coupling $g(h^0XX)$ and the coupling modifier κ_X as follows:

$$\mathrm{DEV(X)} = \mathrm{g(h^0XX)^2} - 1 = \kappa_{\mathrm{X}}^2 - 1. \tag{7}$$

We define the relative deviation of the width ratio $\Gamma(X)/\Gamma(Y)$ from its SM prediction as follows:

$$\mathrm{DEV(X/Y)} \equiv \frac{\Gamma(\mathrm{X})/\Gamma(\mathrm{Y})}{\Gamma(\mathrm{X})_{\mathrm{SM}}/\Gamma(\mathrm{Y})_{\mathrm{SM}}} - 1. \tag{8}$$

Note that we have the following approximation:

$$\mathrm{DEV(X/Y)} \simeq \mathrm{DEV(X)} - \mathrm{DEV(Y)} \quad (\text{for } |\mathrm{DEV(Y)}| \ll 1). \tag{9}$$

It is important to notice that a significant (substantial) part of the experimental systematic and statistical errors of the measured widths $\Gamma(X)$ and $\Gamma(Y)$ cancel out in the width ratio $\Gamma(X)/\Gamma(Y)$, which results in a relatively small experimental error of the measured width ratio. The theoretical errors of the MSSM widths $\Gamma(X)_{\mathrm{MSSM}}$ and $\Gamma(Y)_{\mathrm{MSSM}}$ also cancel out significantly in the width ratio $\Gamma(X)_{\mathrm{MSSM}}/\Gamma(Y)_{\mathrm{MSSM}}$, which leads to a relatively small theoretical error of the MSSM width ratio; e.g., the phase-space factor proportional to $1/m_{h^0}$ cancels out in the MSSM width ratio, where we impose the constraint $m_{h^0} = 125.09 \pm 3.48$ GeV (see Table V). Therefore, the experimental measurement errors as well as the MSSM prediction uncertainties tend to cancel out significantly in the width ratios, making the measurement of these width ratios a very sensitive probe of virtual SUSY loop effects in these h^0 decays at future lepton colliders. Moreover, as we expect from Eq. (9), the deviation of the MSSM width ratio from the SM prediction can be significantly enhanced compared with that of a single MSSM width from the SM; e.g., we will see below that DEV(γ/g) can be as large as about +9% [see Fig. 12(c)]. Furthermore, there can be significant correlations between the deviation of the single MSSM width from the SM value and that of the MSSM width ratio from the SM; e.g., there is a very strong correlation between DEV(c) and DEV(b/c) as shown in Fig. 4(a) below.

2. Scatter plots for fermionic decays

Scatter plots for DEVs of fermionic decays—In Fig. 3, we show the scatter plot in the DEV(c)-DEV(b) plane obtained from the MSSM parameter scan. DEV(c) and DEV(b) can be quite large simultaneously since large trilinear couplings T_{U23}, T_{U32}, and T_{U33} can enhance both DEV(c) and DEV(b) as explained above. From Fig. 3(a), indeed we see that DEV(c) and DEV(b) can be quite large simultaneously: DEV(c) can be as large as $\sim \pm 60\%$ and DEV(b) can be as large as $\sim \pm 20\%$. Future lepton colliders together with HL-LHC can observe such large deviations from SM at very high significance (see Appendix B); e.g., from Appendix B, we see that the expected absolute 1σ error of DEV(c) is sufficiently small $\Delta\mathrm{DEV(c)} = (3.6\%, 2.4\%, 1.8\%)$ and that of DEV(b) is also sufficiently small $\Delta\mathrm{DEV(b)} = (1.7\%, 1.1\%, 0.9\%)$ at (ILC250, ILC250 + 500, ILC250 + 500 + 1000) together with HL-LHC, respectively [see Fig. 3(a)]. The expected absolute 1σ errors of DEV(c) and DEV(b) at the other lepton colliders are similar to those at ILC (see Appendix B).

In Fig. 3(b), we show also the ATLAS and CMS data of DEV(b) at 95% CL obtained from the recent κ_b data [33,34] shown in Table V by using the relation $\mathrm{DEV(b)} = \kappa_b^2 - 1$: $\mathrm{DEV(b)} = -0.21^{+0.44}_{-0.33}$ (95% CL) (ATLAS) and $\mathrm{DEV(b)} = -0.02^{+0.76}_{-0.52}$ (95% CL) (CMS). Here, note that the current LHC data of κ_c [and hence, that of DEV(c) also] has very large uncertainties (errors) [33,34]. We see that both the SM

[7]The SM widths $\Gamma(h^0 \to XX)_{\mathrm{SM}}$ $(X = g, \gamma)$ are computed in Refs. [31,32], but we do not use these SM widths. Instead, we compute the SM widths $\Gamma(h^0 \to XX)_{\mathrm{SM}}$ $(X = g, \gamma)$ at the NLO QCD level by ourselves in order to calculate the relative deviation of the MSSM width $\Gamma(h^0 \to XX)_{\mathrm{MSSM}}$ from the SM width $\Gamma(h^0 \to XX)_{\mathrm{SM}}$ at the NLO QCD level *consistently*. We also compute the SM widths $\Gamma(h^0 \to XX)_{\mathrm{SM}}$ $(X = g, \gamma)$ by taking the decoupling SUSY/Higgs limit of the MSSM width $\Gamma(h^0 \to XX)_{\mathrm{MSSM}}$ at the NLO QCD level. We have found that the former SM widths agree with the latter SM widths very well. We have obtained $\Gamma(h^0 \to gg)_{\mathrm{SM}} = 0.262$ MeV and $\Gamma(h^0 \to \gamma\gamma)_{\mathrm{SM}} = 0.0111$ MeV.

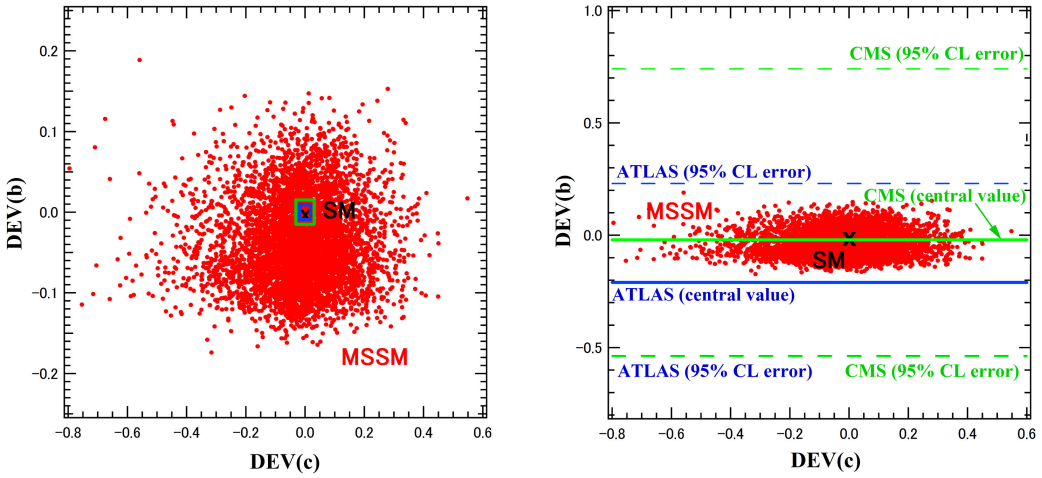

(a) (b)

FIG. 3. Shown in (a) is the scatter plot in the DEV(c)-DEV(b) plane obtained from the MSSM parameter scan described in Sec. III. "X" marks the SM point. The green and blue boxes indicate the expected 1σ errors at ILC250 and ILC250 + 500, respectively (see Table VI). Though in principle the expected 1σ error should be shown by an error ellipse, here, it is shown by an error box as an approximation since such 1σ error ellipse in the κ_c-κ_b plane [and hence, in the DEV(c)-DEV(b) plane] is not given in [20,21]. The expected absolute 1σ errors at the other lepton colliders are similar to those at ILC (see Table VI). In (b), we show also the ATLAS and CMS data of DEV(b) obtained from the recent κ_b data [33,34] by using the DEV(b)-κ_b relation $\mathrm{DEV(b)} = \kappa_b^2$-1.

and the MSSM are consistent with the recent ATLAS and CMS data, and that the errors of the recent ATLAS and CMS data are relatively very large.

In Fig. 4(a), we show the scatter plot in the DEV(b/c)-DEV(c) plane obtained from the MSSM parameter scan described in Sec. III. We see that there is a strong correlation between DEV(b/c) and DEV(c), and that DEV(b/c) can be quite large for large |DEV(c)|: DEV(b/c) can exceed +100% for DEV(c) $\lesssim -0.5$. This strong correlation stems from the fact that the two DEVs have a common origin of enhancement, i.e., the large trilinear couplings $T_{U23,32,33}$. This behavior is consistent with the expectation from the argument above.

In Fig. 4(b), we show the scatter plot in the DEV(b/c)-DEV(b) plane obtained from the MSSM parameter scan. We see that there is an appreciable correlation between DEV(b/c) and DEV(b), which comes also from the fact that the two DEVs have a common origin of enhancement, i.e., the large trilinear couplings $T_{U23,32,33}$ and $T_{D23,32,33}$.

Scatter plots for QFV decay $h^0 \to bs$—As for the explicitly QFV decay $h^0 \to bs$, Refs. [14–18] computed $B(h^0 \to bs)$ in the MSSM with general QFV. However, they neglected LR and RL squark flavor (generation) mixings, which we have found very important. Moreover, the constraints used in [14–18] are incomplete and/or old (obsolete). Reference [19] computed $B(h^0 \to bs)$ at full 1-loop level in the MSSM with general QFV including LL, RR, LR, RL squark flavor (generation) mixings respecting relevant constraints as we do here. However, some of the constraints used in [19] (including those from B meson data) are already obsolete; e.g., they performed a $B(h^0 \to bs)$ contour plot analysis in the squark flavor mixing parameter planes in six benchmark scenarios (S1–S6). All of the benchmark scenarios except S5 are already excluded by the recent gluino mass limit from LHC, $m_{\tilde{g}} > 2.35$ TeV for $m_{\tilde{\chi}_1^0} < 1.55$ TeV (see Appendix A).

In the present work, we update these constraints (including the B meson data) and perform a systematic MSSM parameter scan respecting the updated constraints. Furthermore, we take into account also the expected mass limits for the SUSY particles and the heavier MSSM Higgs bosons H^0, A^0, H^+ from the future HL-LHC experiment. We compute $B(h^0 \to bs)$ approximately from the full 1-loop level width $\Gamma(h^0 \to bs)$ in the MSSM with general QFV by dividing it by the LO total width of the h^0 decay obtained from the public code SPheno-v3.3.8 [27,28].

In Fig. 5, we show the scatter plot in the $B(h^0 \to bs)$-DEV(b) plane obtained from the MSSM parameter scan described in Sec. III. We see that $B(h^0 \to bs)$ can be as large as ~0.1% and that $B(h^0 \to bs)$ and DEV(b) can be sizable simultaneously. This is due to the fact that $B(h^0 \to bs)$ and DEV(b) have a common origin of enhancement, i.e., large trilinear couplings $T_{U23,32,33}$ and $T_{D23,32,33}$ [see Figs. 1(b) and 1(c)].

On the other hand, from our contour plot analysis of the branching ratio $B(h^0 \to bs)$ shown below in Fig. 10(c), we find that it can be as large as ~0.15% respecting all the updated constraints including the expected mass limits for the SUSY particles and the heavier MSSM Higgs bosons from the future HL-LHC experiment. Here, we remark that [19] found that $B(h^0 \to bs)$ can be as large as $\sim O(0.1\%)$,

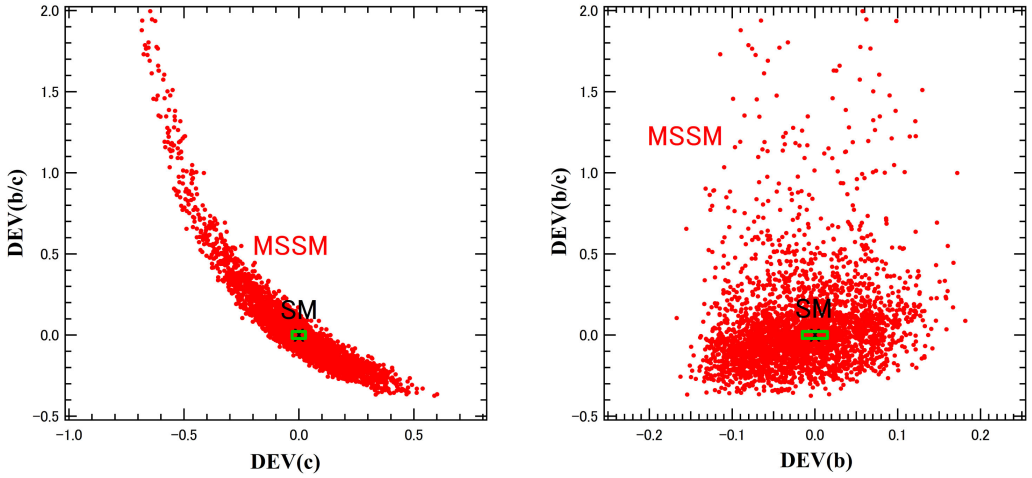

FIG. 4. The scatter plot in the (a) DEV(c)-DEV(b/c) and (b) DEV(b)-DEV(b/c) planes obtained from the MSSM parameter scan described in Sec. III. "X" marks the SM point. The expected absolute 1σ errors at ILC250 shown by the green box are given by $[\Delta\mathrm{DEV(c)}, \Delta\mathrm{DEV(b)}, \Delta\mathrm{DEV(b/c)}] = (3.6\%, 1.7\%, 3.1\%)$ (see Table VI). Though, in principle, the expected 1σ error should be shown by an error ellipse, here, it is shown by an error box as an approximation. The expected absolute 1σ errors at the other lepton colliders are similar to those at ILC (see Table VI).

however, respecting already outdated constraints in the MSSM with general QFV. It is very small [$B(h^0 \to bs) \lesssim 10^{-7}$] in the SM [14,35,36]. The ILC250 + 500 + 1000 sensitivity to this branching ratio $B(h^0 \to bs)$ could be ~0.1% at 4σ signal significance [37] (see also [38]) (see Appendix C). Hence, such QFV decay $h^0 \to bs$ in the MSSM with general QFV can be observed at ILC with very high signal significance.[8] Note that the LHC and HL-LHC sensitivity to this QFV decay branching ratio should not be so good due to huge QCD background [38].

Here, we comment on the effect of resummation of the bottom Yukawa coupling for $\Gamma(h^0 \to b\bar{b})$ and $\Gamma(h^0 \to bs)$ in the MSSM. We have studied the effect of the resummation of the bottom Yukawa coupling for large $\tan\beta$ [41]. It turns out that in our case with large m_{A^0} close to the decoupling Higgs limit (see Table I), the resummation effect (the so-called Δ_b effect) is very small (<0.1%) [5,42].

3. Scatter plots for bosonic decays

Scatter plot in DEV(γ)-DEV(g) *plane*—In Fig. 6, we show the scatter plot in the DEV(γ)-DEV(g) plane obtained from the MSSM parameter scan. We see that there is a strong correlation between DEV(γ) and DEV(g). This correlation is due to the fact that the lighter up-type squark ($\tilde{u}_{1,2,3}$) loop (stop-scharm mixture loop) contributions dominate the two DEVs. From Fig. 6(a), we see that DEV(γ) and DEV(g) can be sizable simultaneously: DEV(γ) can be as large as $\sim \pm 1\%$ and DEV(g) can be as large as $\sim \pm 4\%$. ILC together with HL-LHC can observe such sizable deviation DEV(g) at fairly high significance though they can not observe such moderate deviation DEV(γ) significantly (see Appendix B): The expected absolute 1σ error of DEV(γ) is $\Delta\mathrm{DEV}(\gamma) = (2.4\%, 2.2\%, 2.0\%)$ and that of DEV(g) is $\Delta\mathrm{DEV(g)} = (1.8\%, 1.4\%, 1.1\%)$ at (ILC250, ILC250 + 500, ILC250 + 500 + 1000) together with HL-LHC, respectively [see Fig. 6(a)]. The expected absolute 1σ errors of DEV(γ) and DEV(g) at the other lepton colliders

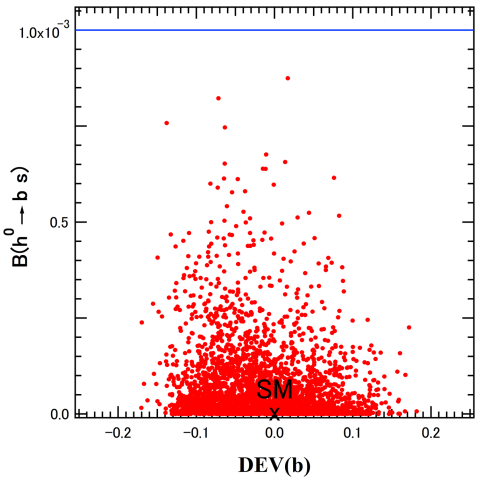

FIG. 5. The scatter plot in the $B(h^0 \to bs)$-DEV(b) plane obtained from the MSSM parameter scan described in Sec. III. The blue horizontal line indicates the ILC250 + 500 + 1000 sensitivity to $B(h^0 \to bs)$ of ~0.1% at 4σ signal significance. "X" marks to the SM point.

[8]The expected upper bound on $B(h^0 \to bs)$ at FCC-ee is [39]: $B(h^0 \to bs) < 4.5 \times 10^{-4}$ (95% CL). The expected upper bound on $B(h^0 \to bs)$ at CEPC is [40]: $B(h^0 \to bs) < 2.2 \times 10^{-4}$ (95% CL).

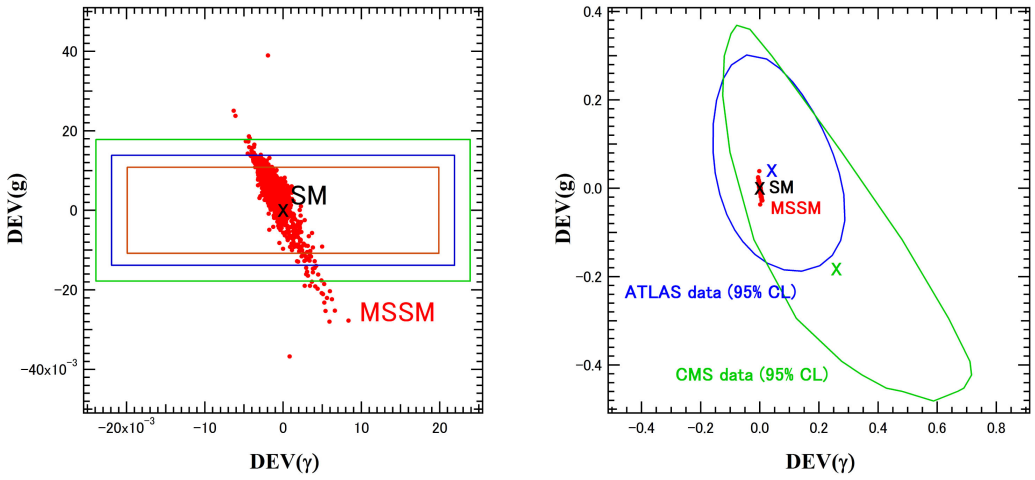

FIG. 6. In (a), we show the scatter plot in the DEV(γ)-DEV(g) plane obtained from the MSSM parameter scan described in Sec. III. "X" marks the SM point. The green, blue, and brown boxes indicate the expected 1σ errors at ILC250, ILC250 + 500, and ILC250 + 500 + 1000, respectively (see Table VI). Though, in principle, the expected 1σ error should be shown by an error ellipse, here it is shown by an error box as an approximation since such 1σ error ellipse in the κ_γ-κ_g plane [and hence, in the DEV(γ)-DEV(g) plane] is not given in [20,21]. The expected absolute 1σ errors at the other lepton colliders are similar to those at ILC (see Table VI). We have confirmed that all the constraints in Appendix A are satisfied at the MSSM parameter points corresponding to the two isolated points with DEV(g) $\sim \pm 4\%$ in (a). In (b), we show also the ATLAS and CMS data of DEV(γ) and DEV(g) at 95% CL obtained from the recent ATLAS and CMS data of κ_γ and κ_g [33,34] by using the relation DEV(X) = κ_X^2-1. The black, blue, and green "X" marks the SM point, and the central values of the ATLAS and CMS data, respectively.

are similar to those at ILC (see Appendix B). It is important to note that DEV(g) can be as large as $\sim -7\%$ as can be seen in the contour plot of Fig. 11(c) in the following, which corresponds to more than 5σ deviation from the SM at ILC250 + 500 and ILC250 + 500 + 1000. We would see this fact if we generate much more MSSM parameter points in our parameter scan.

In Fig. 6(b), we show also the ATLAS and CMS data of DEV(γ) and DEV(g) at 95% CL obtained from the recent ATLAS and CMS data of κ_γ and κ_g [33,34] by using the relation DEV(X) $= \kappa_X^2 - 1$. We see that both the SM and the MSSM are allowed by the recent ATLAS and CMS data and that the errors of the ATLAS and CMS data are too large to distinguish the MSSM from the SM.

C. Contour plot analysis

1. Benchmark scenario

In order to see the relevant MSSM parameter dependence of DEV(b), DEV(c), DEV(b/c), $B(h^0 \to bs)$, DEV(γ), DEV(g), and DEV(γ/g) in more detail, we take a reference scenario P1 where we have sizable DEV(b), DEV(c), DEV (b/c), $B(h^0 \to bs)$, DEV(γ), DEV(g), and DEV(γ/g) and then variate the relevant MSSM parameters around this point P1. All MSSM input parameters for P1 are shown in Table II, where one has DEV(c) $= -0.11$, DEV(b) $= -0.15$, DEV(b/c) $= -0.042$, $B(h^0 \to bs) = 0.040\%$, DEV(γ) $= 0.011$, DEV(g) $= -0.045$ and DEV(γ/g) $= 0.059$. The scenario P1 satisfies all the present experimental and theoretical constraints shown in Appendix A. The resulting physical masses of the particles are shown in Table III. The flavor decompositions of the lighter squarks $\tilde{u}_{1,2,3}$ and $\tilde{d}_{1,2,3}$ are shown in Table IV.

TABLE II. The MSSM parameters for the reference point P1 (in units of GeV or GeV^2 except for $\tan\beta$). All parameters are defined at scale Q = 1 TeV, except m_{A^0}(pole). The parameters that are not shown here are taken to be zero.

$\tan\beta$	M_1	M_2	M_3	μ	m_{A^0}(pole)
33	1660	765	4615	870	5325

M^2_{Q22}	M^2_{Q33}	M^2_{Q23}	M^2_{U22}	M^2_{U33}	M^2_{U23}
3975^2	3160^2	920^2	3465^2	1300^2	795^2

M^2_{D22}	M^2_{D33}	M^2_{D23}	T_{U23}	T_{U32}	T_{U33}
2620^2	2425^2	-1625^2	−2040	−1880	−4945

T_{D23}	T_{D32}	T_{D33}	T_{E33}
−2360	1670	−2395	−300

M^2_{Q11}	M^2_{U11}	M^2_{D11}	M^2_{L11}	M^2_{L22}	M^2_{L33}	M^2_{E11}	M^2_{E22}	M^2_{E33}
4500^2	4500^2	4500^2	1500^2	1500^2	1500^2	1500^2	1500^2	1500^2

TABLE III. Physical masses in GeV of the particles for the scenario of Table II.

$m_{\tilde{\chi}_1^0}$	$m_{\tilde{\chi}_2^0}$	$m_{\tilde{\chi}_3^0}$	$m_{\tilde{\chi}_4^0}$	$m_{\tilde{\chi}_1^+}$	$m_{\tilde{\chi}_2^+}$
781	882	911	1669	782	914

m_{h^0}	m_{H^0}	m_{A^0}	m_{H^+}
124	5325	5325	5359

$m_{\tilde{g}}$	$m_{\tilde{u}_1}$	$m_{\tilde{u}_2}$	$m_{\tilde{u}_3}$	$m_{\tilde{u}_4}$	$m_{\tilde{u}_5}$	$m_{\tilde{u}_6}$
4424	868	3011	3331	3877	4402	4402

$m_{\tilde{d}_1}$	$m_{\tilde{d}_2}$	$m_{\tilde{d}_3}$	$m_{\tilde{d}_4}$	$m_{\tilde{d}_5}$	$m_{\tilde{d}_6}$
1705	2833	3010	3877	4397	4403

$m_{\tilde{\nu}_1}$	$m_{\tilde{\nu}_2}$	$m_{\tilde{\nu}_3}$	$m_{\tilde{l}_1}$	$m_{\tilde{l}_2}$	$m_{\tilde{l}_3}$	$m_{\tilde{l}_4}$	$m_{\tilde{l}_5}$	$m_{\tilde{l}_6}$
1509	1509	1528	1489	1489	1509	1512	1512	1545

For the calculation of the masses and the mixings of the sparticles and the MSSM Higgs bosons, as well as for the low-energy observables, especially those in the B and K meson sectors (see Table V), we use the public code SPheno v3.3.8 [27,28]. As for the effective mixing angle α in the CP even neutral Higgs boson sector, we obtain $\alpha = -0.0303$ with $H^0 = \cos\alpha(\sqrt{2}\mathrm{Re}(H_1^0) - v_1) + \sin\alpha(\sqrt{2}\mathrm{Re}(H_2^0) - v_2)$ and $h^0 = -\sin\alpha(\sqrt{2}\mathrm{Re}(H_1^0) - v_1) + \cos\alpha(\sqrt{2}\mathrm{Re}(H_2^0) - v_2)$. We compute the coupling modifier κ_X by using $\mathrm{DEV(X)} = \kappa_X^2 - 1$ [see Eq. (7)]. We obtain $\kappa_b = 0.922$ ($\mathrm{DEV(b)} = -0.15$), $\kappa_g = 0.977$ ($\mathrm{DEV(g)} = -0.045$), and $\kappa_\gamma = 1.005$ ($\mathrm{DEV}(\gamma) = 0.011$) in the scenario P1, which satisfy the LHC data in Table V. For the other coupling modifiers, and the invisible decay branching ratio B_{inv} and the undetected decay branching ratio B_{und}, see Appendix D.

Furthermore, we have confirmed that in all contour plots shown below the red hatched regions (which include always our reference point P1) satisfy all the constraints in Appendix A and also all the expected sparticle mass limits and (m_{A^0}, $\tan\beta$) limit from the negative search for the sparticles and the MSSM Higgs bosons H^0, A^0, $H^\pm$ in the future HL-LHC experiments [43–49]. In this confirmation, we have used contour plots of all the sparticle masses in the individual parameter plane.

TABLE IV. Flavor decompositions of the mass eigenstates $\tilde{u}_{1,2,3}$ and $\tilde{d}_{1,2,3}$ for the scenario of Table II. Shown are the expansion coefficients of the mass eigenstates in terms of the flavor eigenstates. Imaginary parts of the coefficients are negligibly small.

	$\tilde{u}_L$	$\tilde{c}_L$	$\tilde{t}_L$	$\tilde{u}_R$	$\tilde{c}_R$	$\tilde{t}_R$
$\tilde{u}_1$	0.0001	−0.0190	−0.0959	0	0.0767	−0.9922
$\tilde{u}_2$	−0.0283	−0.0736	0.9740	0	0.1978	−0.0775
$\tilde{u}_3$	0.0088	0.0288	−0.1886	0	0.9771	0.0932

	$\tilde{d}_L$	$\tilde{s}_L$	$\tilde{b}_L$	$\tilde{d}_R$	$\tilde{s}_R$	$\tilde{b}_R$
$\tilde{d}_1$	0	−0.0012	0.0099	0	0.6585	0.7525
$\tilde{d}_2$	0	−0.0058	0.0448	0	−0.7521	0.6575
$\tilde{d}_3$	−0.0018	−0.1183	0.9919	0	0.0274	−0.0373

Here, concerning the constraint from the negative searches for the MSSM Higgs bosons at LHC, we remark the following point: In all contour plots, m_{A^0} is fixed to be $\simeq$5.3 TeV and hence, $m_{H^0,A^0,H^+} \simeq 5.3$ TeV for which H^0, A^0, H^+ are obviously too heavy to be produced at LHC (13 TeV) and HL-LHC(14 TeV). Here, note that $m_{H^0} \simeq m_{A^0} \simeq m_{H^+}$ in the decoupling Higgs limit in the MSSM. Hence, the entire contour plot planes are allowed by the negative search for the MSSM Higgs bosons H^0, A^0, $H^\pm$ at LHC(13 TeV) and HL-HLC(14 TeV).

2. Contour plots for fermionic decays

In Fig. 7, we show contours of DEV(b) around the benchmark point P1 in various parameter planes. Figure 7(a) shows contours of DEV(b) in the T_{U23}-T_{U32} plane. We see that |DEV(b)| increases quickly with the increase of $|T_{U23}|$ and $|T_{U32}|$ as expected. We also see that it is large ($-0.18 \lesssim \mathrm{DEV(b)} \lesssim -0.13$) respecting all the constraints in a significant part of this parameter plane. From Fig. 7(b), we see that DEV(b) is also sensitive to T_{U33} and can be as large as ~ -0.18. As can be seen in Fig. 7(c), DEV(b) is fairly sensitive to M^2_{U23}, especially for large $|T_{U32}| \gtrsim 3$ TeV, as expected, and is large ($-0.18 \lesssim \mathrm{DEV(b)} \lesssim -0.15$) respecting all the constraints in a significant part of this parameter plane.

As for the contours of DEV(b) around P1 in the planes of down-type squark parameters T_{D23}, T_{D32}, T_{D33}, and M^2_{D23}, we have found that DEV(b) is rather insensitive to these parameters as expected: the weaker dependence of DEV(b) on the down-type squark parameters such as T_{D23} than that on the up-type squark parameters such as T_{U23} stems from the fact that the $\tilde{d}_{1,2,3}$-$\tilde{g}$ loops [Fig. 1(c)] are less important than the $\tilde{u}_{1,2,3}$-$\tilde{\chi}^\pm_{1,2}$ loops [Fig. 1(b)] mainly due to the small $\mathrm{Re}(H_1^0)$ component of h^0 in our decoupling Higgs scenario, which suppresses the $h^0 - \tilde{d}_i - \tilde{d}_j$ couplings.

As shown in Table VI, the expected absolute 1σ error of DEV(b) measured at ILC is given by $\Delta\mathrm{DEV(b)} = (1.7\%, 1.1\%, 0.9\%)$ at (ILC250, ILC250 + 500, ILC250 + 500 + 1000) and similar results are obtained for the future lepton colliders other than ILC. Therefore, such large deviation DEV(b) ($\sim -15\%$ to -20%) in the sizable region allowed by all the constraints (including the expected sparticle and MSSM Higgs boson mass limits from HL-LHC) as shown in Fig. 7 can be observed with very high significance at the future lepton colliders such as ILC.

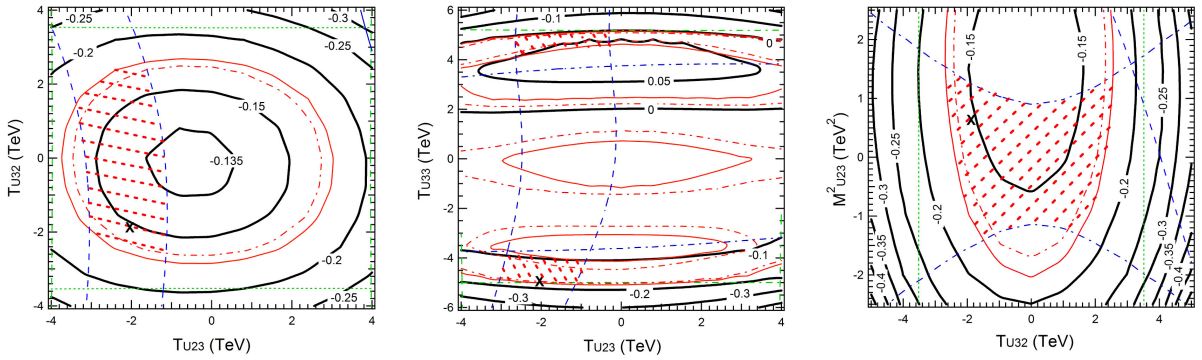

FIG. 7. Contour plots of DEV(b) around the benchmark point P1 in the parameter planes of (a) $T_{U23} - T_{U32}$, (b) $T_{U23} - T_{U33}$, and (c) $T_{U32} - M^2_{U23}$. The parameters other than the shown ones in each plane are fixed as in Table II. The "X" marks P1 in the plots. The red hatched region satisfies all the constraints in Appendix A and also all the expected sparticle mass limits and $(m_{A^0}, \tan\beta)$ limit at 95% CL from a negative search for sparticles and the heavier MSSM Higgs bosons H^0, A^0, $H^\pm$ in the future HL-LHC experiments [43–49]. The red solid lines, green dashed lines, green dotted lines, green dash-dotted lines, blue solid lines, blue dashed lines, and blue dash-dotted lines show the m_{h^0} bound, vacuum stability bound for T_{U23}, T_{U32}, T_{U33}, $B(b \to s\gamma)$ bound, $B(B_s \to \mu^+\mu^-)$ bound, and $m_{\tilde{u}_1}$ bound, respectively. Just for reference, the red dash-dotted lines show the m_{h^0} bounds for a hypothetical case that the total theoretical error is ± 2 GeV instead of ± 3 GeV; i.e., the contours of m_{h^0} (GeV) $= 125.09 + (0.48 + 2) = 127.57$ and $m_{h^0}(\text{GeV}) = 125.09 - (0.48 + 2) = 122.61$. We see that only a small part of the red hatched region is excluded by this hypothetical m_{h^0} bounds.

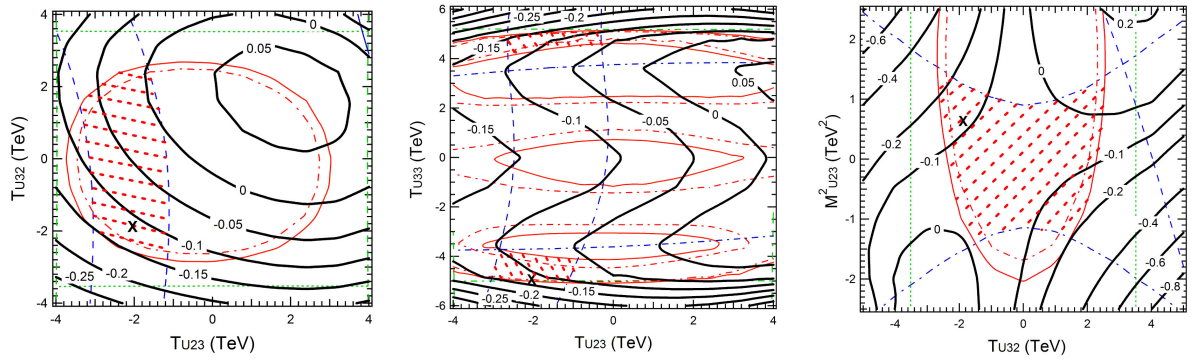

FIG. 8. Contour plots of DEV(c) around the benchmark point P1 in the parameter planes of (a) $T_{U23} - T_{U32}$, (b) $T_{U23} - T_{U33}$, and (c) $T_{U32} - M^2_{U23}$. The parameters other than the shown ones in each plane are fixed as in Table II. The "X" marks P1 in the plots. The definitions of the red hatched regions and the bound lines are the same as those in Fig. 7.

Just to show how the allowed parameter region is affected by the change of the total theoretical error of m_{h^0}, we have drawn m_{h^0} bound lines in the contour plots of DEVs and $B(h^0 \to bs)$ in the hypothetical case that the total theoretical error is ± 2 GeV instead of ± 3 GeV. As can be seen in Figs. 7–8 and 10–12, the allowed parameter region is only a little affected by the change of the total theoretical error.

In Fig. 8, we show contour plots of DEV(c) around the benchmark point P1 in various parameter planes. Figure 8(a) shows contours of DEV(c) in the T_{U23}-T_{U32} plane. We see that DEV(c) is sensitive to T_{U23} and T_{U32}: |DEV(c)| quickly increases with the increase of T_{U23} and T_{U32} as expected [see Fig. 1(a) and the related argument above]. We find also that DEV(c) is sizable $(-0.15 \lesssim \text{DEV(c)} \lesssim -0.05)$ respecting all the constraints in a significant part of this parameter plane. From Fig. 8(b), we see that DEV(c) is sensitive also to T_{U33}, quickly increases with the increase of $|T_{U33}|$ as expected, and it is large $(-0.20 \lesssim \text{DEV(c)} \lesssim -0.05)$ respecting all the constraints in a sizable part of this parameter plane. As can be seen in Fig. 8(c), DEV(c) is sensitive to T_{U32} and M^2_{U23} increasing with the increase of T_{U32} and M^2_{U23} as expected and is quite large $(-0.25 \lesssim \text{DEV(c)} \lesssim 0.1)$ respecting all the constraints in a significant part of this parameter plane. Note that DEV(c) is especially large for the large product $T_{U32} \times M^2_{U23} (< 0)$. This is due to the following reason:

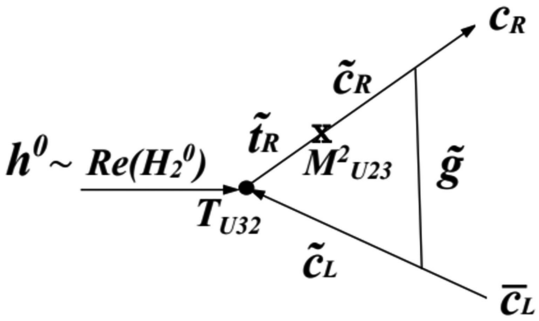

FIG. 9. The leading gluino loop contribution to the decay amplitude for $h^0 \to c\bar{c}$ in terms of the MI approximation.

(i) The gluino loop contribution [Fig. 1(a)] to the decay amplitude for $h^0 \to c\bar{c}$ can be very large positive or negative for a large value of the product $T_{U32} \times M^2_{U23}$ since the leading gluino loop contribution is proportional to the product $T_{U32} \times M^2_{U23}$ in terms of the mass-insertion (MI) approximation (see Fig. 9) [5].

(ii) Hence, the interference term between the tree diagram and the gluino loop contribution of Fig. 1(a) can be very large (positive or negative) for a large value of the product $T_{U32} \times M^2_{U23}$, which can lead to even *negative* width $\Gamma(h^0 \to c\bar{c})$ at one-loop level. In this case, the perturbation theory breaks down.

(iii) Therefore, in principle, the deviation of $\Gamma(h^0 \to c\bar{c})$ from the SM value [DEV(c)] can be very large for a large value of the product $T_{U32} \times M^2_{U23}$.

As for the contours of DEV(c) around P1 in the planes of down-type squark parameters T_{D23}, T_{D32}, T_{D33}, and M^2_{D23}, we have found that DEV(c) is insensitive to these parameters as expected: the main MSSM 1-loop corrections to $\Gamma(h^0 \to c\bar{c})$ stem from $\tilde{u}_{1,2,3}$-$\tilde{g}$ loops [see Fig. 1(a)], which do not involve the down-type squark parameters. As shown in Table VI, the expected absolute 1σ error of DEV(c) measured at ILC is given by $\Delta\text{DEV(c)} = (3.6\%, 2.4\%, 1.8\%)$ at (ILC250, ILC250 + 500, ILC250 + 500 + 1000) and similar results are obtained for the future lepton colliders other than ILC. Hence, such large deviation DEV(c) ($\sim +10\%$ to -25%) in the sizable region allowed by all the constraints (including the expected sparticle mass limits from HL-LHC) as shown in Fig. 8 can be observed with very high significance at the future lepton colliders such as ILC.

In Fig. 10, we show contours of $B(h^0 \to bs)$ around the benchmark point P1 in various parameter planes. Figure 10(a) shows contours of $B(h^0 \to bs)$ in the T_{U23}-T_{U32} plane. We see that $B(h^0 \to bs)$ is sensitive to both T_{U23} and T_{U32}, increases with the increase of $|T_{U23}|$ and $|T_{U32}|$, as expected [see Fig. 1(b)], and can be as large as about 0.00045 in the allowed region. From Fig. 10(b), we see that $B(h^0 \to bs)$ is also sensitive to T_{U33}, increases with the increase of $|T_{U33}|$, as expected, and can be as large as about 0.0006 in the allowed region. From Fig. 10(c), we find that $B(h^0 \to bs)$ is also sensitive to $\tan\beta$ as expected and can be as large as about 0.0015 in the allowed region. We also see that it is sizable $[0.00025 \lesssim B(h^0 \to bs) \lesssim 0.0015]$ respecting all the constraints in a significant part of this parameter plane. From Fig. 10(d), we see that $B(h^0 \to bs)$ is sensitive to both T_{D23} and T_{D32} (being the $\tilde{s}_R - \tilde{b}_L$ and $\tilde{s}_L - \tilde{b}_R$ mixing parameter, respectively), increases with the increase of $|T_{D23}|$ and $|T_{D32}|$ (with $T_{D23} \times T_{D32} < 0$), as expected, and can reach 0.001 in the allowed region.

The 4σ signal significance sensitivity to $B(h^0 \to bs)$ of ILC250 + 500 + 1000 is $B(h^0 \to bs) = 0.001$ as mentioned above. Hence, such large $B(h^0 \to bs)$ ($\sim$0.001 to 0.0015) in the region allowed by all the constraints (including the expected sparticle mass limits from HL-LHC) as shown in Fig. 10 can be observed at ILC with high significance.

3. Contour plots for bosonic decays

In Fig. 11, we show contour plots of DEV(g) around the benchmark point P1 in various parameter planes. Figure 11(a) shows contours of DEV(g) in the T_{U23}-T_{U32} plane. We see that DEV(g) is fairly sensitive to T_{U23} and T_{U32} as expected [see Fig. 2(a) and the related argument above]. It is sizable ($-0.05 \lesssim \text{DEV(g)} \lesssim -0.044$) in the allowed region. From Fig. 11(b), we see that DEV(g) is also sensitive to T_{U33} increasing quickly with the increase of $|T_{U33}|$ as expected. As can be seen in Fig. 11(c), DEV(g) is sensitive to M^2_{U23} increasing with the increase of $|M^2_{U23}|$ as expected from decreasing $m_{\tilde{u}_1}$ for increasing $|M^2_{U23}|$, and it is sizable ($-0.07 \lesssim \text{DEV(g)} \lesssim -0.045$) in the allowed region.

As for the contours of DEV(g) around P1 in the planes of the down-type squark parameters T_{D23}, T_{D32}, T_{D33}, and M^2_{D23}, we have found that DEV(g) is insensitive to these parameters as expected.

As shown in Table VI, the expected absolute 1σ error of DEV(g) measured at ILC is given by $\Delta\text{DEV(g)} = (1.8\%, 1.4\%, 1.1\%)$ at (ILC250, ILC250 + 500, ILC250 + 500 + 1000), and similar results are obtained for the future lepton colliders other than ILC. Hence, such large deviation DEV(g) ($\sim -4\%$ to -7%) in the sizable region allowed by all the constraints (including the expected sparticle mass limits from HL-LHC) as shown in Fig. 11 can be observed with high significance at the future lepton colliders such as ILC.

As for contour plots of DEV(γ) around the benchmark point P1, we have found that the tendency of them is similar to that of DEV(g), except the overall normalization and sign. This is due to the fact that, as can be seen in Fig. 6(a), for any MSSM parameter point, approximately we have (see Ref. [6] also)

$$\text{DEV}(\gamma) \sim -\frac{1}{4}\text{DEV(g)}. \tag{10}$$

In Fig. 12, we show contour plots of DEV(γ/g) around the benchmark point P1 in various parameter planes. Figure 12(a) shows contours of DEV(γ/g) in the

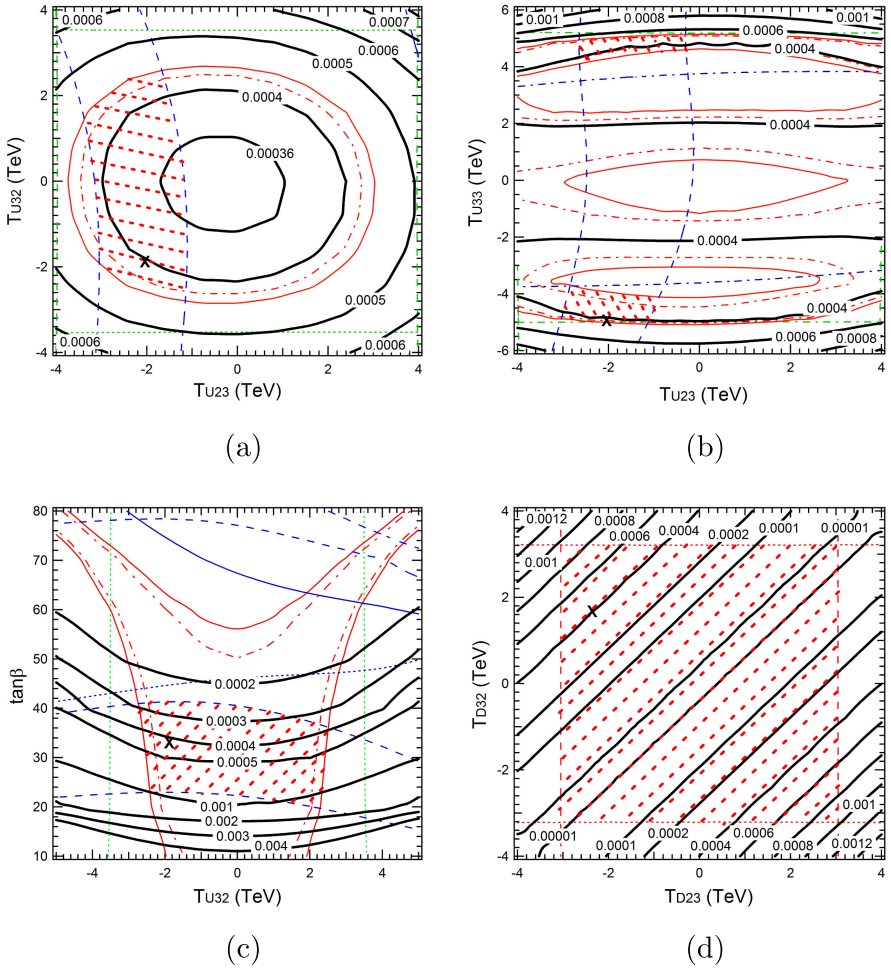

FIG. 10. Contour plots of $B(h^0 \to bs)$ around the benchmark point P1 in the parameter planes of (a) $T_{U23} - T_{U32}$, (b) $T_{U23} - T_{U33}$, (c) $T_{U32} - \tan\beta$, and (d) $T_{D23} - T_{D32}$. The parameters other than the shown ones in each plane are fixed as in Table II. The "X" marks P1 in the plots. Note that 4σ signal significance sensitivity to $B(h^0 \to bs)$ of ILC250 + 500 + 1000 is $B(h^0 \to bs) = 0.001$. The definitions of the red hatched regions and the bound lines are the same as those in Fig. 7. In addition to these the blue dotted lines, the red dashed lines and red dotted lines show the ΔM_{B_s} bound, and the vacuum stability bound for T_{D23} and T_{D32}, respectively. In Figs. 10(a)–10(c), we see that only a small part of the red hatched region is excluded by the hypothetical m_{h^0} bounds mentioned in Fig. 7. The entire region of Fig. 10(d) is allowed by the hypothetical m_{h^0} bounds.

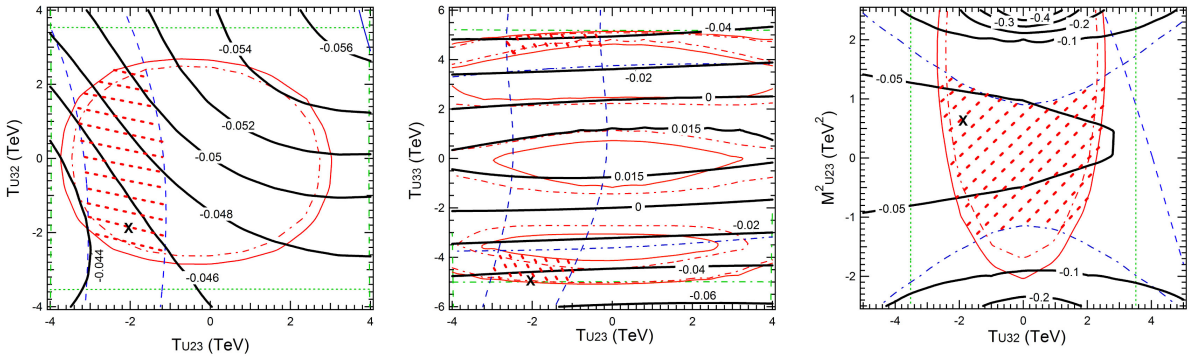

FIG. 11. Contour plots of DEV(g) around the benchmark point P1 in the parameter planes of (a) $T_{U23} - T_{U32}$, (b) $T_{U23} - T_{U33}$, and (c) $T_{U32} - M^2_{U23}$. The parameters other than the shown ones in each plane are fixed as in Table II. The "X" marks P1 in the plots. The definitions of the red hatched regions and the bound lines are the same as those in Fig. 7.

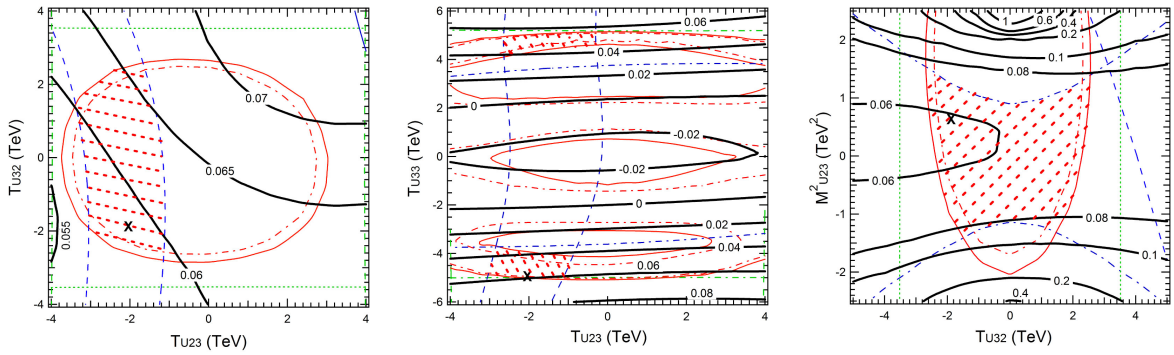

(a) (b) (c)

FIG. 12. Contour plots of DEV(γ/g) around the benchmark point P1 in the parameter planes of (a) $T_{U23} - T_{U32}$, (b) $T_{U23} - T_{U33}$, and (c) $T_{U32} - M^2_{U23}$. The parameters other than the shown ones in each plane are fixed as in Table II. The "X" marks P1 in the plots. The definitions of the red hatched regions and the bound lines are the same as those in Fig. 7.

T_{U23}-T_{U32} plane. We see that DEV(γ/g) is fairly sensitive to T_{U23} and T_{U32} as expected (see Fig. 2 and the related argument above). It is sizable ($0.06 \lesssim \mathrm{DEV}(\gamma/\mathrm{g}) \lesssim 0.07$) in the allowed region. From Fig. 12(b), we see that DEV(γ/g) is also sensitive to T_{U33}, quickly increases with increase of $|T_{U33}|$ as expected. As can be seen in Fig. 12(c), DEV(γ/g) is also sensitive to M^2_{U23} increasing with the increase of $|M^2_{U23}|$ as expected from decreasing $m_{\tilde{u}_1}$ for increasing $|M^2_{U23}|$, and it is large ($0.06 \lesssim \mathrm{DEV}(\gamma/\mathrm{g}) \lesssim 0.09$) in the allowed region. As for the contours of DEV(γ/g) around P1 in the planes of down-type squark parameters T_{D23}, T_{D32}, T_{D33}, and M^2_{D23}, we have found that DEV(γ/g) is insensitive to these parameters as expected.

As shown in Table VI, the expected absolute 1σ error of DEV(γ/g) measured at ILC is given by $\Delta\mathrm{DEV}(\gamma/\mathrm{g}) = (3.3\%, 2.8\%, 2.3\%)$ at (ILC250, ILC250 + 500, ILC250 + 500 + 1000), and similar results are obtained for the future lepton colliders other than ILC. Therefore, such a large deviation DEV(γ/g) ($\sim +6\%$ to $+9\%$) in the sizable region allowed by all the constraints (including the expected sparticle mass limits from HL-LHC) as shown in Fig. 12 can be observed with fairly high significance at the future lepton colliders such as ILC.

D. Theoretical errors of the MSSM prediction for DEVs

Before closing this section, we comment briefly on the theoretical error of the MSSM prediction $\mathrm{DEV(X)_{MSSM}}$. We find that, in general, the theoretical error of the MSSM prediction $\mathrm{DEV(X)_{MSSM}}$ tends to be significantly small compared with the expected experimental error of the DEV (X) measured at the future lepton colliders [4,6]. The theoretical error of the MSSM prediction $\mathrm{DEV(X)_{MSSM}}$ comes from two sources. One is the parametric uncertainty, and the other is the renormalization scale-dependence uncertainty. The former is due to the errors of the SM input parameters, such as $\alpha_s^{\overline{\mathrm{MS}}}(m_Z)$ and the latter is due to unknown higher order corrections. The main reason of this tendency is as follows: the theoretical errors (the parametric errors and the scale-dependence errors) of $\Gamma(X)_{\mathrm{MSSM}}$ and $\Gamma(X)_{\mathrm{SM}}$ significantly cancel out in the ratio $\Gamma(X)_{\mathrm{MSSM}}/\Gamma(X)_{\mathrm{SM}}$ in the MSSM prediction $\mathrm{DEV(X)_{MSSM}} = \Gamma(X)_{\mathrm{MSSM}}/\Gamma(X)_{\mathrm{SM}} - 1$, resulting in a significantly small theoretical error of $\mathrm{DEV(X)_{MSSM}}$. Here, note that we compute the SM widths $\Gamma(X)_{\mathrm{SM}}$ by taking the decoupling SUSY/Higgs limit of the MSSM width $\Gamma(X)_{\mathrm{MSSM}}$.

For example, as for the MSSM prediction $\mathrm{DEV(g)_{MSSM}}$ at the benchmark point P1, by using the theoretical error estimation method described in [6], we find that the parametric absolute 1σ error is 0.073% and the scale-dependence absolute error is 0.080%. Hence, we find the total theoretical absolute 1σ error of the MSSM prediction of DEV(g) at P1 is 0.153% (= 0.073% + 0.080%) by adding the parametric absolute 1σ error to the scale-dependence absolute error linearly. On the other hand, the expected experimental absolute 1σ error of DEV(g) is 1.8%, 1.4%, 1.1% at ILC250, ILC250 + 500, ILC250 + 500 + 1000 together with HL-LHC, respectively (see Table VI). Therefore, we find that indeed the theoretical error of the MSSM prediction of DEV(g) is significantly small compared with the expected experimental error of DEV(g) measured at the future lepton colliders such as ILC.

V. SUMMARY AND CONCLUSION

We have studied the decays $h^0(125) \to c\bar{c}, b\bar{b}, b\bar{s}, \gamma\gamma, gg$ in the MSSM with general QFV due to squark generation mixings. *In strong contrast to* the usual studies in the MSSM with minimal flavor violation, we have found that the deviations of these MSSM decay widths from the SM values can be quite sizable. *For the first time*, we have performed a systematic MSSM parameter scan for these

decay widths respecting all relevant theoretical and experimental constraints. From the parameter scan, we have found the following:

(1) DEV(c) and DEV(b) can be very large simultaneously: DEV(c) can be as large as $\sim \pm 60\%$, and DEV(b) can be as large as $\sim \pm 20\%$ (see Fig. 3).
(2) DEV(b/c) can exceed $\sim +100\%$ (see Fig. 4).
(3) $B(h^0 \to bs)$ can be as sizable as ~0.15% exceeding the ILC250 + 500 + 1000 sensitivity of ~0.1% at 4σ signal significance [see Fig. 10(c)].
(4) DEV(γ) and DEV(g) can be sizable simultaneously: DEV(γ) can become $\sim \pm 1\%$, and DEV(g) can be as large as $\sim +4\%$ and $\sim -7\%$ [see Figs. 6 and 11(c)].
(5) DEV(γ/g) can be as large as $\sim +9\%$ [see Fig. 12(c)].
(6) There are significant correlations among these DEVs and $B(h^0 \to bs)$:
   (a) There is a very strong correlation between DEV (b/c) and DEV(c) [see Fig. 4(a)].
   (b) There is a significant correlation between $B(h^0 \to bs)$ and DEV(b) (see Fig. 5).
   (c) There is a very strong correlation between DEV(γ) and DEV(g). This correlation is due to the fact that the $\tilde{u}_{1,2,3}$-loop contributions dominate in the two DEVs (see Fig. 6).
(7) We have pointed out that the experimental measurement uncertainties as well as the MSSM prediction uncertainties tend to cancel out significantly in the width ratios, making the measurement of these width ratios a very sensitive probe of virtual SUSY loop effects in these h^0 decays at future lepton colliders.
(8) All of these sizable deviations in the h^0 decays are due to (i) large scharm-stop mixing and large scharm/stop involved trilinear couplings $T_{U23}, T_{U32}, T_{U33}$, (ii) large sstrange-sbottom mixing and large sstrange/sbottom involved trilinear couplings T_{D23}, T_{D32}, T_{D33}, and (iii) large bottom Yukawa coupling Y_b for large $\tan\beta$ and large top Yukawa coupling Y_t.

Such sizable deviations from the SM can be observed at high signal significance in future lepton colliders such as ILC, CLIC, CEPC, FCC-ee, and MuC *even after* the failure of SUSY particle discovery at the HL-LHC. In case the deviation pattern shown here is really observed at the lepton colliders, then it would strongly suggest the discovery of QFV SUSY (the MSSM with general QFV).

ACKNOWLEDGMENTS

We would like to thank Werner Porod for helpful discussions, especially for the permanent support concerning SPheno. We also thank Junping Tian and Jorge de Blas for supplying us helpful information on the experiments at the future lepton colliders, especially at ILC. We also thank Sven Heinemeyer for helpful discussions.

APPENDIX A: THEORETICAL AND EXPERIMENTAL CONSTRAINTS

The experimental and theoretical constraints taken into account in the present work are discussed in detail in [61]. Here, we list the updated constraints from K and B physics and those on the Higgs boson mass and couplings in Table V. For the mass of the Higgs boson h^0, taking the combination of the ATLAS and CMS measurements $m_{h^0} = 125.09 \pm 0.24$ GeV [59] and adding the theoretical uncertainty of $\sim \pm 3$ GeV [60] linearly to the experimental uncertainty at 2σ, we take $m_{h^0} = 125.09 \pm 3.48$ GeV. Here, we remark that the uncertainty of $\sim \pm 3$ GeV is the intrinsic theoretical error due to unknown higher-order corrections (i.e., the error due to renormalization scheme/scale dependence). It is well known that the parametric uncertainties due to the experimental errors of the SM input parameters [such as m_t, $\alpha_s(m_Z)$, …] are also important [62,63]. The dominant source of the parametric uncertainties is the experimental error of the top quark mass m_t [63] since the radiative corrected m_{h^0} is very sensitive to m_t in the MSSM. Therefore, the total theoretical error given by the sum of the intrinsic theoretical error and the parametric errors should be significantly larger than ± 3 GeV. Here, we take ± 3 GeV as the total theoretical error, conservatively. It is important to note that the parametric errors, especially that due to experimental error of the top quark mass, remain to be significant even if the intrinsic theoretical error is improved to be very small.

The h^0 couplings that receive SUSY QFV effects significantly are $g(hbb)$ [5], $g(hcc)$ [4], $g(hgg)$, and $g(h\gamma\gamma)$ [6].[9] The measurement of $g(hcc)$ is very difficult due to the huge QCD background at LHC; there is no significant experimental data on $g(hcc)$ at this time. Hence, the relevant h^0 couplings to be compared with the LHC observations are $g(hbb)$, $g(hgg)$, and $g(h\gamma\gamma)$. Therefore, we list the LHC data on $g(hbb)$ (κ_b), $g(hgg)$ (κ_g), and $g(h\gamma\gamma)$ (κ_γ) in Table V.

As the constraints from the decays $B \to D^{(*)}\tau\nu$ are unclear due to large theoretical uncertainties [4],[10] we do not take these constraints into account in our paper. As the issues of possible anomalies of $R(D^{(*)}) = B(B \to D^{(*)}\tau\nu)/B(B \to D^{(*)}\ell\nu)$ with $\ell = e$ or μ are not yet settled [66], we do not take the constraints from these ratios into account either. Note that the possible related anomaly of

[9]Precisely speaking, in principle, $g(htt)$ coupling could also receive SUSY QFV effects significantly. However, predicting the effective coupling $g(htt)$ at loop levels in the MSSM is very difficult since its theoretical definition in the context of $t\bar{t}h$ production at LHC is unclear [64].

[10]As pointed out in [65], the theoretical predictions (in the SM and MSSM) on $\mathrm{B}(B \to Dl\nu)$ and $\mathrm{B}(B \to D^*l\nu)$ ($l = \tau, \mu, e$) have potentially large theoretical uncertainties due to the theoretical assumptions on the hadronic form factors at the BDW^+ and BD^*W^+ vertices (also at the BDH^+ and BD^*H^+ vertices in the MSSM). Hence, the constraints from these decays are unclear.

TABLE V. Constraints on the MSSM parameters from the K- and B-meson data relevant mainly for the mixing between the second and the third generations of squarks and from the data on the h^0 mass and couplings κ_b, κ_g, κ_γ. The fourth column shows constraints at 95% CL obtained by combining the experimental error quadratically with the theoretical uncertainty, except for $B(K_L^0 \to \pi^0\nu\bar{\nu})$, m_{h^0} and $\kappa_{b,g,\gamma}$.

Observable	Experimental data	Theoretical uncertainty	Constraint (95% CL)
$10^3 \times \lvert\epsilon_K\rvert$	2.228 ± 0.011 (68% CL) [25]	± 0.28 (68% CL) [50]	2.228 ± 0.549
$10^{15} \times \Delta M_K$ [GeV]	3.484 ± 0.006 (68% CL) [25]	± 1.2 (68% CL) [50]	3.484 ± 2.352
$10^9 \times \mathrm{B}(K_L^0 \to \pi^0\nu\bar{\nu})$	<3.0 (90% CL) [25]	± 0.002 (68% CL) [25]	<3.0 (90% CL)
$10^{10} \times \mathrm{B}(K^+ \to \pi^+\nu\bar{\nu})$	1.7 ± 1.1 (68% CL) [25]	± 0.04 (68% CL) [25]	$1.7^{+2.16}_{-1.70}$
ΔM_{B_s} [ps^{-1}]	17.757 ± 0.021 (68% CL) [25,51]	± 2.7 (68% CL) [52]	17.757 ± 5.29
$10^4 \times \mathrm{B}(b \to s\gamma)$	3.32 ± 0.15 (68% CL) [25,51]	± 0.23 (68% CL) [53]	3.32 ± 0.54
$10^6 \times \mathrm{B}(b \to s l^+ l^-)$ ($l = e$ or μ)	$1.60^{+0.48}_{-0.45}$ (68% CL) [54]	± 0.11 (68% CL) [55]	$1.60^{+0.97}_{-0.91}$
$10^9 \times \mathrm{B}(B_s \to \mu^+\mu^-)$	$2.69^{+0.37}_{-0.35}$ (68% CL) [56]	± 0.23 (68% CL) [57]	$2.69^{+0.85}_{-0.82}$
$10^4 \times \mathrm{B}(B^+ \to \tau^+\nu)$	1.06 ± 0.19 (68% CL) [51]	± 0.29 (68% CL) [58]	1.06 ± 0.69
m_{h^0} [GeV]	125.09 ± 0.24(68%CL) [59]	± 3 [60]	125.09 ± 3.48
κ_b	$0.89^{+0.22}_{-0.21}$(95%CL) [33]		$0.89^{+0.22}_{-0.21}$ (ATLAS)
	$0.99^{+0.33}_{-0.31}$(95%CL) [34]		$0.99^{+0.33}_{-0.31}$ (CMS)
κ_g	$0.95^{+0.14}_{-0.13}$(95%CL) [33]		$0.95^{+0.14}_{-0.13}$ (ATLAS)
	0.92 ± 0.16(95%CL) [34]		0.92 ± 0.16 (CMS)
κ_γ	1.01 ± 0.12(95%CL) [33]		1.01 ± 0.12 (ATLAS)
	1.10 ± 0.16(95%CL) [34]		1.10 ± 0.16 (CMS)

$R_{K^{(*)}} = B(B \to K^{(*)}e^+e^-)/B(B \to K^{(*)}\mu^+\mu^-)$ is gone away now [67].

In [26], the QFV decays $t \to qh^0$ with $q = u$, c, have been studied in the MSSM with general QFV. It is found that these decays cannot be visible at the current and high luminosity LHC runs due to the very small decay branching ratios $\mathrm{B}(t \to qh^0)$, giving no significant constraint on the $\tilde{c} - \tilde{t}$ and $\tilde{s} - \tilde{b}$ mixings.

In [68], the QFV decay branching ratio $B(Z^0 \to bs) \equiv B(Z^0 \to b\bar{s}) + B(Z^0 \to \bar{b}s)$ was studied in the MSSM with general QFV. It was shown that the current best experimental upper limit on $B(Z^0 \to bs)$ gives no significant constraint on the $\tilde{s} - \tilde{b}$ and $\tilde{c} - \tilde{t}$ mixings.[11]

We comment on the recent data on the anomalous magnetic moment of the muon a_μ from the Fermilab experiment [70]. The Fermilab data result in 5.0σ discrepancy between the experimental data and the SM prediction [71].[12] In our scenario with heavy sleptons/sneutrinos with masses of about 1.5 TeV, the MSSM loop contributions to a_μ are so small that they can not explain the discrepancy between the new data and the SM prediction. Therefore, in the context of our scenario, this discrepancy should be explained by the loop contributions of another new physics coexisting with SUSY.

We also comment on the recent W boson mass data from CDF II [75], which is about $+7\sigma$ away from the SM prediction. However, the CDF II data disagree significantly with the world average of the m_W data from the other experiments [69].[13] This issue of the m_W data is not yet settled. Hence, we do not take into account this m_W constraint on the MSSM parameters in our analysis.

In addition to these, we also require our scenarios to be consistent with the following experimental constraints:

(i) The LHC limits on sparticle masses (at 95% CL) [80–84]:

We impose conservative limits for safety though actual limits are somewhat weaker than those shown here. In the context of simplified models, gluino masses $m_{\tilde{g}} \lesssim 2.35$ TeV are excluded for $m_{\tilde{\chi}_1^0} < 1.55$ TeV. There is no gluino mass limit for $m_{\tilde{\chi}_1^0} > 1.55$ TeV. The eightfold degenerate first two generation squark masses are excluded below 1.92 TeV for $m_{\tilde{\chi}_1^0} < 0.9$ TeV. There is no limit on

[11]Note that no experimental upper limit on $B(Z^0 \to bs)$ is listed in PDG2022 [69].

[12]On the other hand, Refs. [72–74] point to agreement of the SM prediction with the current experimental data.

[13]We remark the caveats from Refs. [76,77]: According to the PDG prescription, the new "scale-factored" world average of m_W data including the CDF II data is $+3.2\sigma$ off the SM value used by CDF II. We also note that the new improved ATLAS m_W data [78] is consistent with their old data [79] and the previous world average [69].

the masses for $m_{\tilde{\chi}_1^0} > 0.9$ TeV. We impose this squark mass limit on $m_{\tilde{u}_3}$ and $m_{\tilde{d}_3}$. Bottom-squark masses are excluded below 1.26 TeV for $m_{\tilde{\chi}_1^0} < 0.73$ TeV. There is no bottom-squark mass limit for $m_{\tilde{\chi}_1^0} > 0.73$ TeV. Here, the bottom-squark mass means the lighter sbottom mass $m_{\tilde{b}_1}$. We impose this limit on $m_{\tilde{d}_1}$ since $\tilde{d}_1 \sim \tilde{b}_R$ (see Table IV). A typical top-squark mass lower limit is ~1.26 TeV for $m_{\tilde{\chi}_1^0} < 0.62$ TeV. There is no top-squark mass limit for $m_{\tilde{\chi}_1^0} > 0.62$ TeV. Here, the top-squark mass means the lighter stop mass $m_{\tilde{t}_1}$. We impose this limit on $m_{\tilde{u}_1}$ since $\tilde{u}_1 \sim \tilde{t}_R$ (see Table IV). For sleptons/sneutrinos heavier than the lighter chargino $\tilde{\chi}_1^\pm$ and the second neutralino $\tilde{\chi}_2^0$, the mass limits are $m_{\tilde{\chi}_1^\pm}, m_{\tilde{\chi}_2^0} > 0.74$ TeV for $m_{\tilde{\chi}_1^0} \lesssim 0.3$ TeV, and there is no $m_{\tilde{\chi}_1^\pm}$, $m_{\tilde{\chi}_2^0}$ limits for $m_{\tilde{\chi}_1^0} > 0.3$ TeV; for sleptons/sneutrinos lighter than $\tilde{\chi}_1^\pm$ and $\tilde{\chi}_2^0$, the mass limits are $m_{\tilde{\chi}_1^\pm}, m_{\tilde{\chi}_2^0} > 1.15$ TeV for $m_{\tilde{\chi}_1^0} \lesssim 0.72$ TeV, and there is no $m_{\tilde{\chi}_1^\pm}$, $m_{\tilde{\chi}_2^0}$ limits for $m_{\tilde{\chi}_1^0} > 0.72$ TeV. For mass degenerate selectrons $\tilde{e}_{L,R}$ and smuons $\tilde{\mu}_{L,R}$, masses below 0.7 TeV are excluded for $m_{\tilde{\chi}_1^0} < 0.41$ TeV. For mass degenerate staus $\tilde{\tau}_L$ and $\tilde{\tau}_R$, masses below 0.39 TeV are excluded for $m_{\tilde{\chi}_1^0} < 0.14$ TeV. There is no sneutrino $\tilde{\nu}$ mass limit from LHC yet. Sneutrino masses below 94 GeV are excluded by LEP200 experiment [25].

(ii) The constraint on $(m_{A^0,H^+}, \tan\beta)$ (at 95% CL) from the negative searches for the MSSM Higgs bosons H^0, A^0, and H^+ at LHC [85–95], where H^0 is the heavier CP-even neutral Higgs boson and H^+ is the charged Higgs boson: The $(m_{A^0,H^+}, \tan\beta)$ limit from the negative search for the heavier MSSM Higgs bosons H^0, A^0, and H^+ at LHC depends on the MSSM scenarios (such as hMSSM scenario, M_h^{125} scenario, …). However, from [85–95], we find that in general the $(m_{A^0,H^+}, \tan\beta)$ limits of ATLAS/CMS are rather insensitive to the choice of the MSSM scenarios. Here, note that $m_{H^0} \simeq m_{A^0} \simeq m_{H^+}$ in the decoupling Higgs scenarios as ours. From ATLAS/CMS data [85–95], especially [93], we find that the $(m_{A^0}, \tan\beta)$ limit from the negative search for the decay $H^0/A^0 \to \tau^+\tau^-$ [as shown in Fig. 2(c) of [85]] is most important for $\tan\beta > 10$. The $(m_{A^0}, \tan\beta)$ limit (at 95% CL) shown in Fig. 2(c) of [85] is the strongest for $\tan\beta > 10$ among those obtained in [85–95]. Therefore, we take and respect this strongest $(m_{A^0}, \tan\beta)$ limit in our parameter scan analysis for $\tan\beta > 10$.

(iii) The experimental limit on SUSY contributions on the electroweak ρ parameter [96]: $\Delta\rho(\mathrm{SUSY}) < 0.0012$.

Furthermore, we impose the following theoretical constraints from the vacuum stability conditions for the trilinear coupling matrices [97]:

$$|T_{U\alpha\alpha}|^2 < 3Y_{U\alpha}^2(M_{Q\alpha\alpha}^2 + M_{U\alpha\alpha}^2 + m_2^2), \tag{A1}$$

$$|T_{D\alpha\alpha}|^2 < 3Y_{D\alpha}^2(M_{Q\alpha\alpha}^2 + M_{D\alpha\alpha}^2 + m_1^2), \tag{A2}$$

$$|T_{U\alpha\beta}|^2 < Y_{U\gamma}^2(M_{Q\beta\beta}^2 + M_{U\alpha\alpha}^2 + m_2^2), \tag{A3}$$

$$|T_{D\alpha\beta}|^2 < Y_{D\gamma}^2(M_{Q\beta\beta}^2 + M_{D\alpha\alpha}^2 + m_1^2), \tag{A4}$$

where $\alpha,\beta = 1,2,3, \alpha \neq \beta; \gamma = \mathrm{Max}(\alpha,\beta)$, and $m_1^2 = (m_{H^+}^2 + m_Z^2 \sin^2\theta_W)\sin^2\beta - \frac{1}{2}m_Z^2$, $m_2^2 = (m_{H^+}^2 + m_Z^2 \times \sin^2\theta_W)\cos^2\beta - \frac{1}{2}m_Z^2$. The Yukawa couplings of the up-type and down-type quarks are $Y_{U\alpha} = \sqrt{2}m_{u_\alpha}/v_2 = \frac{g}{\sqrt{2}}\frac{m_{u_\alpha}}{m_W \sin\beta}$ $(u_\alpha = u,c,t)$ and $Y_{D\alpha} = \sqrt{2}m_{d_\alpha}/v_1 = \frac{g}{\sqrt{2}}\frac{m_{d_\alpha}}{m_W \cos\beta}$ $(d_\alpha = d,s,b)$, with m_{u_α} and m_{d_α} being the running quark masses at the scale Q = 1 TeV and g being the SU(2) gauge coupling. All soft SUSY-breaking parameters are given at Q = 1 TeV. As SM parameters we take $m_Z = 91.2$ GeV and the on shell top-quark mass $m_t = 172.9$ GeV [25].

APPENDIX B: EXPECTED EXPERIMENTAL ERRORS OF THE DEVIATIONS DEVS AND THE EFFECTIVE HIGGS COUPLINGS AT FUTURE LEPTON COLLIDERS

Here, we summarize expected experimental *absolute* 1σ errors of the deviations DEV(X) and DEV(X/Y) measured at future lepton colliders.

According to Eq. (7), the expected *absolute* 1σ error of the relative deviation DEV(X) denoted by $\Delta\mathrm{DEV(X)}$ is related with the expected *relative* 1σ error of the effective coupling $g(h^0XX)$ denoted by $\delta g(h^0XX)$ as follows:

$$\Delta\mathrm{DEV(X)} \simeq 2\delta g(h^0XX). \tag{B1}$$

In Table VI, we show the expected *absolute* 1σ errors of the measured deviations DEV(X) and DEV(X/Y) denoted by $\Delta\mathrm{DEV(X)}$ and $\Delta\mathrm{DEV(X/Y)}$ at future lepton colliders. The errors $\Delta\mathrm{DEV(X)}$ are obtained by using Eq. (B1) and the expected *relative* 1σ error of the effective coupling $\delta g(h^0XX)$ given in Table 29 of Ref. [21].[14] The errors $\Delta\mathrm{DEV(X/Y)}$ are obtained according to Ref. [98].

[14]The expected *relative* 1σ errors of the effective couplings $\delta g(h^0XX)$ given in Table 7 of Ref. [20] are similar to those given in Table 29 of Ref. [21].

TABLE VI. The expected *absolute* 1σ error of the deviations DEV(X) and DEV(X/Y) [denoted by $\Delta\mathrm{DEV(X)}$ and $\Delta\mathrm{DEV(X/Y)}$] measured at future lepton colliders: ILC-I = ILC250 + Giga-Z, ILC-II = ILC250 + 500 + Giga-Z, ILC-III = ILC250 + 500 + 1000 + Giga-Z; CLIC-I = CLIC380, CLIC-II = CLIC380 + 1500, CLIC-III = CLIC380 + 1500 + 3000; FCC-ee I = FCC-ee240 + Z/WW, FCC-ee II = FCC-ee240 + 365 + Z/WW; CEPC-I = CEPC240 + Z/WW, CEPC-II = CEPC240 + 360 + Z/WW; MuC-I = MuC3 TeV, MuC-II = MuC10 TeV, MuC-III = MuC10 TeV + 125 GeV. As for ILC, the results without Giga-Z run are almost identical to those with Giga-Z one. The Z/WW denote Z-pole and WW threshold runs. All results except for MuC-I and MuC-II are those from the free-Γ_H fit and the results for MuC-I and MuC-II are those from the constrained-Γ_H fit, where Γ_H is the total width of the Higgs boson h^0. The details of run scenarios of the lepton colliders are explained in Ref. [21]. The HL-LHC and LEP/SLD measurements are combined with all lepton collider run scenarios.

	ILC-I	ILC-II	ILC-III	CLIC-I	CLIC-II	CLIC-III
$\Delta\mathrm{DEV(b)}$	1.7%	1.1%	0.9%	2.2%	1.2%	1.1%
$\Delta\mathrm{DEV(c)}$	3.6%	2.4%	1.8%	8.6%	3.8%	3.0%
$\Delta\mathrm{DEV}(\gamma)$	2.4%	2.2%	2.0%	2.6%	2.4%	2.2%
$\Delta\mathrm{DEV(g)}$	1.8%	1.4%	1.1%	2.2%	1.6%	1.4%
$\Delta\mathrm{DEV(b/c)}$	3.1%	2.1%	1.3%	8.2%	3.5%	2.5%
$\Delta\mathrm{DEV}(\gamma/\mathrm{g})$	3.3%	2.8%	2.3%	3.4%	3.1%	2.6%

	FCC-ee I	FCC-ee II	CEPC-I	CEPC-II	MuC-I	MuC-II	MuC-III
$\Delta\mathrm{DEV(b)}$	1.3%	1.2%	0.86%	0.84%	1.8%	0.92%	1.1%
$\Delta\mathrm{DEV(c)}$	2.8%	2.6%	2.4%	2.2%	12.4%	3.8%	3.6%
$\Delta\mathrm{DEV}(\gamma)$	2.4%	2.2%	1.8%	1.8%	2.4%	1.4%	1.5%
$\Delta\mathrm{DEV(g)}$	1.5%	1.4%	0.9%	0.88%	1.7%	0.92%	1.0%
$\Delta\mathrm{DEV(b/c)}$	2.2%	2.1%	2.0%	1.9%	11.9%	3.5%	3.4%
$\Delta\mathrm{DEV}(\gamma/\mathrm{g})$	3.0%	2.9%	2.1%	2.0%	3.2%	1.6%	1.6%

APPENDIX C: ILC SENSITIVITY TO THE BRANCHING RATIO $B(h^0 \to bs)$

The setup conditions for this ILC sensitivity are as follows [37]:

(1) The signal is the QFV decay $h^0 \to b\bar{q}$ and $h^0 \to \bar{b}q$ with the light quark $q = d/s$. The dominant background is the QFC decay $h^0 \to b\bar{b}$, where either b jet or $\bar{b}$ jet is misidentified as a light quark-jet (a q jet). We consider the case $B(h^0 \to bq) \equiv B(h^0 \to b\bar{q}) + B(h^0 \to \bar{b}q) = 0.1\%$ and take $B(h^0 \to b\bar{b}) = 58\%$.

(2) As for the efficiencies, the followings are assumed: The optimal b-tagging efficiency for a b jet, $\epsilon_{b/b}$ is ∼94%. The q-tagging efficiency for a q jet, $\epsilon_{q/q}$ is ∼90%. The q-tagging efficiency for a b jet, $\epsilon_{q/b}$ is ∼6%. The b-tagging efficiency for a q jet, $\epsilon_{b/q}$ is ∼10%. The efficiency of other selection cuts, $\epsilon_{\mathrm{other}}$ is assumed to be around 70%, such as that from Higgs mass cut, Z mass cut, angular cuts, etc., which would be needed to suppress background events other than $h^0 \to b\bar{b}$. This 70% efficiency would be common for the signal $h^0 \to bq$ and the dominant background $h^0 \to b\bar{b}$.

(3) Regarding the amount of accumulated data at ILC, the specifications of the H-20 scenario [99] (see also [21,100]) are adopted basically;

(a) ILC250 stage; The total number of h^0 production events $N^{h^0}_{\mathrm{tot}}$ is assumed to be $\sim 0.5 \times 10^6$, for which the expected significance of the signal $h^0 \to bq$, σ_{sig} is $\sim 2\sigma$ in case $B(h^0 \to bq) = 0.1\%$: $\sigma_{\mathrm{sig}} = N_{\mathrm{sig}}/\sqrt{N_{\mathrm{sig}} + N_{bg}} \sim 2$, where $N_{\mathrm{sig}} = N^{h^0}_{\mathrm{tot}} \cdot B(h^0 \to bq) \cdot \epsilon_{b/b} \cdot \epsilon_{q/q} \cdot \epsilon_{\mathrm{other}} \sim 300$ and $N_{bg} = N^{h^0}_{\mathrm{tot}} \cdot B(h^0 \to b\bar{b}) \cdot 2 \cdot \epsilon_{b/b} \cdot \epsilon_{q/b} \cdot \epsilon_{\mathrm{other}} \sim 23000$.

Alternatively, one can say that the expected upper bound on the branching ratio of the QFV decay, $h^0 \to b\ d/s$, at 95% CL, is 0.1%: $B(h^0 \to b\ d/s) < 0.1\%$ (95% CL) at ILC250.

(b) ILC250 + 500 stage; The total number of h^0 production events $N^{h^0}_{\mathrm{tot}}$ is increased from $\sim 0.5 \times 10^6$ to $\sim 1.1 \times 10^6$, for which the expected significance of the signal $h^0 \to bq$, σ_{sig} is $\sim 3\sigma$ in case $B(h^0 \to bq) = 0.1\%$.

(c) ILC250 + 500 + 1000 stage; The total number of h^0 production events $N^{h^0}_{\mathrm{tot}}$ is further increased from $\sim 1.1 \times 10^6$ to $\sim 2.3 \times 10^6$, for which the expected significance of the signal $h^0 \to bq$, σ_{sig} is $\sim 4\sigma$ in case $B(h^0 \to bq) = 0.1\%$.

APPENDIX D: COUPLING MODIFIERS κ_X, B_{inv}, and B_{und}

Here, we show that the leading-order (LO) coupling modifiers κ_X (X = W, Z, t, τ, μ, Zγ), B_{inv} and B_{und} at the benchmark scenario P1 satisfy the corresponding LHC data [33,34]. In Table VII, we show the LO coupling modifiers

TABLE VII. In this Table, we show the LO coupling modifiers κ_X (X = W, Z, t, τ, μ, Zγ), $B_{\rm inv}$ and $B_{\rm und}$ in the benchmark scenario P1 and the corresponding LHC data at 95% CL [33,34].

X	κ_X at P1	κ_X (95% CL) (ATLAS)	κ_X (95% CL) (CMS)
W	0.9999999986	$1.054^{+0.117}_{-0.116}$	1.02 ± 0.16
Z	0.9999999986	0.993 ± 0.111	1.04 ± 0.14
t	0.9999983786	$0.944^{+0.218}_{-0.214}$	$1.01^{+0.22}_{-0.20}$
τ	1.0017641128	$0.929^{+0.143}_{-0.137}$	0.92 ± 0.16
μ	1.0017641128	$1.063^{+0.482}_{-0.595}$	$1.12^{+0.41}_{-0.43}$
$Z\gamma$	0.98351169	$1.377^{+0.607}_{-0.720}$	$1.65^{+0.67}_{-0.73}$

B_X	B_X at P1	B_X upper bound (95% CL) (ATLAS)	B_X upper bound (95% CL) (CMS)
$B_{\rm inv}$	0.00283	$B_{\rm inv} < 0.13$	$B_{\rm inv} < 0.17$
$B_{\rm und}$	0	$B_{\rm und} < 0.12$	$B_{\rm und} < 0.16$

κ_X (X = W, Z, t, τ, μ, Zγ), $B_{\rm inv}$ and $B_{\rm und}$ at P1 and the corresponding ATLAS/CMS data at 95% CL [33,34].

We compute the LO κ_X (X = W, Z, t, τ, μ) using the LO formulas given in [101,102], in which we input α and β values at P1: $\alpha = -0.03034721$ and $\beta = \tan^{-1}(33) = 1.54050257$; e.g., $\kappa_W = \kappa_Z = \sin(\beta-\alpha) = \sin(1.54050257-(-0.03034721)) = 0.99999999857$. We compute the LO $\kappa_{Z\gamma}$ at P1 using our own Fortran code [103].[15] We compute the LO $B_{\rm inv}$ and $B_{\rm und}$ at P1 using the public code SPheno v3.3.8 [27,28].[16] From Table VII, we find that the LO coupling modifiers κ_X (X = W, Z, t, τ, μ, Zγ), $B_{\rm inv}$ and $B_{\rm und}$ at P1 satisfy the corresponding LHC data at 95% CL [33,34].

Similarly, we have confirmed that the LO coupling modifiers κ_X (X = W, Z, t, τ, μ, Zγ), $B_{\rm inv}$ and $B_{\rm und}$ at all the survival points in our MSSM parameter scan satisfy the corresponding LHC data at 95% CL [33,34].

[15]We compute the LO MSSM width $\Gamma(h^0 \to Z\gamma)_{\rm MSSM}$ at the full 1-loop level at P1 in the MSSM with general QFV and the LO SM width $\Gamma(h^0 \to Z\gamma)_{\rm SM}$ at the full 1-loop level in the SM using our own Fortran code [103]. We obtain the LO $\kappa_{Z\gamma} = 0.98351169$ using $\kappa^2_{Z\gamma} = \Gamma(h^0 \to Z\gamma)_{\rm MSSM}/\Gamma(h^0 \to Z\gamma)_{\rm SM}$.

[16]We compute $B_{\rm inv}$ and $B_{\rm und}$ at P1 using SPheno v3.3.8 as follows: $B_{\rm inv} = B(h^0 \to Z\nu\bar{\nu})B(Z \to \nu\bar{\nu}) = 0.01413 \cdot 0.20 = 0.00283$. $B_{\rm und} = B(h^0 \to$ undetected new physics particles$) = B(h^0 \to$ sparticles$) = 0$ as the LSP neutralino mass $m_{\tilde{\chi}^0_1} = 781$ GeV at P1.

[1] G. Aad *et al.* (ATLAS Collaboration), Phys. Lett. B **716**, 1 (2012).
[2] S. Chatrchyan *et al.* (CMS Collaboration), Phys. Lett. B **716**, 30 (2012).
[3] T. Barklow, K. Fujii, S. Jung, R. Karl, J. List, T. Ogawa, M. E. Peskin, and J. Tian, Phys. Rev. D **97**, 053003 (2018).
[4] A. Bartl, H. Eberl, E. Ginina, K. Hidaka, and W. Majerotto, Phys. Rev. D **91**, 015007 (2015).
[5] H. Eberl, E. Ginina, A. Bartl, K. Hidaka, and W. Majerotto, J. High Energy Phys. 06 (2016) 143.
[6] H. Eberl, K. Hidaka, and E. Ginina, Int. J. Mod. Phys. A **34**, 1950120 (2019).
[7] M. Cahill-Rowley, J. Hewett, A. Ismail, and T. Rizzo, Phys. Rev. D **90**, 095017 (2014).
[8] M. Endo, T. Moroi, and M. Nojiri, J. High Energy Phys. 04 (2015) 176.
[9] A. Arbey *et al.*, Phys. Rev. D **106**, 055002 (2022).
[10] J. Dickinson *et al.*, arXiv:2207.05103.
[11] T. Bose *et al.*, arXiv:2209.13128.
[12] M. Narain *et al.*, arXiv:2211.11084.
[13] A. Brignole, Nucl. Phys. **B898**, 644 (2015).
[14] S. Bejar, F. Dilme, J. Guasch, and J. Sola, J. High Energy Phys. 08 (2004) 018.
[15] A. Curiel, M. Herrero, and D. Temes, Phys. Rev. D **67**, 075008 (2003).
[16] D. Demir, Phys. Lett. B **571**, 193 (2003).
[17] A. Curiel, M. Herrero, W. Hollik, F. Merz, and S. Peñaranda, Phys. Rev. D **69**, 075009 (2004).
[18] G. Barenboim, C. Bosch, J. Lee, M. López-Ibáñez, and O. Vives, Phys. Rev. D **92**, 095017 (2015).
[19] M. E. Gómez, S. Heinemeyer, and M. Rehman, Phys. Rev. D **93**, 095021 (2016).
[20] Jorge de Blas *et al.*, J. High Energy Phys. 01 (2020) 139.
[21] Jorge de Blas *et al.*, arXiv:2206.08326.
[22] M. Cepeda *et al.*, CERN Yellow Rep. Monogr. **7**, 221 (2019).
[23] B. C. Allanach *et al.*, Comput. Phys. Commun. **180**, 8 (2009).

[24] F. Gabbiani, E. Gabrielli, A. Masiero, and L. Silvestrini, Nucl. Phys. **B477**, 321 (1996).
[25] P. A. Zyla *et al.* (Particle Data Group), Prog. Theor. Exp. Phys. **2020**, 083C01 (2020).
[26] A. Dedes *et al.*, J. High Energy Phys. 11 (2014) 137.
[27] W. Porod, Comput. Phys. Commun. **153**, 275 (2003).
[28] W. Porod and F. Staub, Comput. Phys. Commun. **183**, 2458 (2012).
[29] For details, see SPheno home page: https://spheno.hepforge.org/.
[30] D. M. Pierce *et al.*, Nucl. Phys. **B491**, 3 (1997).
[31] D. de Florian *et al.* (LHC Higgs Cross Section Working Group), CERN Yellow Rep. Monogr. **2**, 1 (2017).
[32] L. G. Almeida, S. J. Lee, S. Pokorski, and J. D. Wells, Phys. Rev. D **89**, 033006 (2014).
[33] G. Aad *et al.* (ATLAS Collaboration), Nature (London) **607**, 52 (2022); **612**, E24 (2022).
[34] A. Tumasyan *et al.* (CMS Collaboration), Nature (London) **607**, 60 (2022); A. M. Sirunyan *et al.* (CMS Collaboration), J. High Energy Phys. 07 (2021) 027.
[35] L. G. Benitez-Guzman *et al.*, J. Phys. G **42**, 085002 (2015).
[36] J. F. Kamenik *et al.*, Phys. Rev. D **109**, L011301 (2024).
[37] Junping Tian (private communication).
[38] D. Barducci and A. J. Helmboldt, J. High Energy Phys. 12 (2017) 105.
[39] M. Selvaggi, Talk at FCC Physics Performance Meeting (2024), https://indico.cern.ch/event/1392261/.
[40] H. Liang, Y. Zhu, Y. Wang, Y. Che, C. Zhou, H. Qu, and M. Ruan, Phys. Rev. Lett. **132**, 221802 (2024); M. Ruan, *Plenary Talk at Higgs2023 Conference, 2023, Beijing*, https://indico.ihep.ac.cn/event/18025/contributions/133704/attachments/74198/90943/Physics%20of%20Higgs%20factory%20-%20v2.pdf.
[41] M. Carena *et al.*, Nucl. Phys. **B577**, 88 (2000); J. Guasch *et al.*, Phys. Rev. D **68**, 115001 (2003).
[42] E. Ginina, A. Bartl, H. Eberl, K. Hidaka, and W. Majerotto, Proc. Sci., EPS-HEP2015 (**2016**) 146 [arXiv:1510.03714].
[43] X. Cid Vidal *et al.*, CERN Yellow Rep: Monogr. **7**, 585 (2019), https://e-publishing.cern.ch/index.php/CYRM/article/view/953/770.
[44] T. Bose *et al.*, arXiv:2209.13128.
[45] ATLAS Collaboration, ATLAS Notes ATL-PHYS-PUB-2012-001, ATL-PHYS-PUB-2013-002, ATL-PHYS-PUB-2014-010, and ATL-PHYS-PUB-2018-048.
[46] C. M. Berggren, *Talk at The European Physical Society Conference on High Energy Physics (EPS-HEP2023)* (Hamburg, Germany, 2023), https://indico.desy.de/event/34916/contributions/147692/attachments/83876/111001/berggren-eps-hep-susy-aug23.pdf.
[47] H. Gilmer, Proc. Sci. ICHEP2020 (**2021**) 247, https://indico.cern.ch/event/868940/contributions/3815948/attachments/2081333/3495936/ICHEP_2020-Gilmer.pdf.
[48] M. Narain *et al.*, arXiv:2211.11084.
[49] H. Bahl, P. Bechtle, S. Heinemeyer, S. Liebler, T. Stefaniak, and G. Weiglein, Eur. Phys. J. C **80**, 916 (2020).
[50] J. Brod and M. Gorbahn, Phys. Rev. Lett. **108**, 121801 (2012).
[51] Y. Amhis *et al.* (Heavy Flavor Averaging Group (HFLAV) Collaboration), Eur. Phys. J. C **81**, 226 (2021).
[52] T. Jubb, M. Kirk, A. Lenz, and G. Tetlalmatzi-Xolocotzi, Nucl. Phys. **B915**, 431 (2017); M. Artuso, G. Borissov, and A. Lenz, Rev. Mod. Phys. **88**, 045002 (2016).
[53] M. Misiak *et al.*, Phys. Rev. Lett. **114**, 221801 (2015).
[54] J. P. Lees *et al.* (*BABAR* Collaboration), Phys. Rev. Lett. **112**, 211802 (2014).
[55] T. Huber, T. Hurth, and E. Lunghi, Nucl. Phys. **B802**, 40 (2008).
[56] Y. Amhis, Proc. Sci., ICHEP2020 (2021) 3, https://cds.cern.ch/record/2727203/files/ICHEP_Yasmine.pdf.
[57] C. Bobeth *et al.*, Phys. Rev. Lett. **112**, 101801 (2014).
[58] J. M. Roney, Int. J. Mod. Phys. A **29**, 1430048 (2014).
[59] ATLAS and CMS Collaborations, Phys. Rev. Lett. **114**, 191803 (2015).
[60] S. Borowka, T. Hahn, S. Heinemeyer, G. Heinrich, and W. Hollik, Eur. Phys. J. C **75**, 424 (2015).
[61] H. Eberl, E. Ginina, and K. Hidaka, Eur. Phys. J. C **77**, 189 (2017).
[62] B. C. Allanach, A. Djouadi, J. L. Kneur, W. Porod, and P. Slavich, J. High Energy Phys. 09 (2004) 044.
[63] T. Hahn, S. Heinemeyer, W. Hollik, H. Rzehak, and G. Weiglein, Phys. Rev. Lett. **112**, 141801 (2014).
[64] P. Wu *et al.*, Phys. Lett. B **618**, 209 (2005); S. Dittmaier *et al.*, Phys. Rev. D **90**, 035010 (2014).
[65] U. Nierste, S. Trine, and S. Westhoff, Phys. Rev. D **78**, 015006 (2008).
[66] C. Lazzeroni, *Plenary Talk at The European Physical Society Conference on High Energy Physics (EPS-HEP2023)* (Hamburg, 2023), https://indico.desy.de/event/34916/contributions/142205/attachments/83911/111164/EPS_Lazzeroni_final.pdf.
[67] LHCb Collaboration, Phys. Rev. Lett. **131**, 051803 (2023).
[68] D. Atwood, S. Bar-Shalom, G. Eilam, and A. Soni, Phys. Rev. D **66**, 093005 (2002).
[69] R. L. Workman *et al.* (Particle Data Group), Prog. Theor. Exp. Phys. **2022**, 083C01 (2022) and 2023 update.
[70] D. P. Aguillard *et al.* (The Muon g-2 Collaboration), Phys. Rev. Lett. **131**, 161802 (2023).
[71] T. Aoyama *et al.*, Phys. Rep. **887**, 1 (2020).
[72] S. Borsanyi *et al.*, Nature (London) **593**, 51 (2021).
[73] G. Venanzoni, *Plenary Talk at The European Physical Society Conference on High Energy Physics (EPS-HEP2023)* (Hamburg, 2023), https://pos.sissa.it/449/037/.
[74] F. V. Ignatov *et al.* (CMD-3 Collaboration), Phys. Rev. D **109**, 112002 (2024).
[75] T. Aaltonen *et al.* (CDF Collaboration), Science **376**, 170 (2022).
[76] G. Wilson, Talk at ECFA Higgs Factory Seminars: Precision Physics in the $e^+e^- \to W^+W^-$ Region (2022), https://indico.cern.ch/event/1163667/.
[77] S. Heinemeyer, Talk at IDT-WG3-Phys Open Meeting on m_W (2022), https://agenda.linearcollider.org/event/9357/.
[78] ATLAS Collaboration, ATLAS Note ATLAS-CONF-2023-004, https://cds.cern.ch/record/2853290; M. Schott, Talk at 57th Recontres de Moriond—Electroweak Interactions and Unified Theories, La Thuile (2023).

[79] ATLAS Collaboration, Eur. Phys. J. C **78**, 110 (2018).
[80] F. Moortgat, Proc. Sci., LeptonPhoton2019 (**2019**), https://indico.cern.ch/event/688643/contributions/3410366/attachments/1891440/3120151/LeptonPhoton_SUSY_Filip.pdf.
[81] C. Botta, Proc. Sci. ICHEP2020 (**2021**) 6, https://indico.cern.ch/event/868940/contributions/3905701/attachments/2084745/3502248/ICHEP2020_SUSYOverview_CBotta.pdf; S. Alderweireldt, Proc. Sci. ICHEP2020 (**2021**) 224, https://indico.cern.ch/event/868940/contributions/3815895/attachments/2083268/3499407/ATLAS_EWKSUSY_SAlderweireldt.pdf.
[82] ATLAS Collaboration, ATLAS PUB Note, SUSY May 2020 Summary Plot Update, Report No. ATL-PHYS-PUB-2020-013; See also the following Web Page: Summary plots from the ATLAS Supersymmetry physics group, https://atlas.web.cern.ch/Atlas/GROUPS/PHYSICS/CombinedSummaryPlots/SUSY/.
[83] See the following Web Page: Run 2 Summary plots—13 TeV, https://twiki.cern.ch/twiki/bin/view/CMSPublic/PhysicsResultsSUS#Run_2_Summary_plots_13_TeV.
[84] ATLAS Collaboration, J. High Energy Phys. 02 (2021) 143.
[85] ATLAS Collaboration, Phys. Rev. Lett. **125**, 051801 (2020).
[86] CMS Collaboration, J. High Energy Phys. 09 (2018) 007.
[87] ATLAS Collaboration, J. High Energy Phys. 11 (2018) 085.
[88] ATLAS Collaboration, J. High Energy Phys. 06 (2021) 145.
[89] ATLAS Collaboration, J. High Energy Phys. 09 (2018) 139.
[90] CMS Collaboration, J. High Energy Phys. 01 (2020) 096.
[91] CMS Collaboration, J. High Energy Phys. 07 (2019) 142.
[92] ATLAS Collaboration, J. High Energy Phys. 11 (2024) 097.
[93] ATLAS Note, ATL-PHYS-PUB-2024-008, Summary Plots for Beyond SM Higgs boson searches at ATLAS (See Fig. 1(a)).
[94] ATLAS Collaboration, Phys. Rev. D **111**, 072006 (2025).
[95] CMS Collaboration, J. High Energy Phys. 07 (2023) 073.
[96] G. Altarelli, R. Barbieri, and F. Caravaglios, Int. J. Mod. Phys. A **13**, 1031 (1998).
[97] J. A. Casas and S. Dimopoulos, Phys. Lett. B **387**, 107 (1996).
[98] Private communication with Jorge de Blas who computed the expected relative 1σ errors of the measured width ratios $\Gamma(X)/\Gamma(Y)$ denoted by $\delta[\Gamma(X)/\Gamma(Y)]$ at future lepton colliders by using the same program code as that used in Ref. [21], where $\Gamma(X) \equiv \Gamma(h^0 \to X\bar{X})$. The expected experimental absolute 1σ errors $\Delta\mathrm{DEV(X/Y)}$ at future lepton colliders are obtained by using the following relation: $\Delta\mathrm{DEV(X/Y)} \simeq \delta[\Gamma(X)/\Gamma(Y)]$.
[99] T. Barklow *et al.*, arXiv:1506.07830.
[100] I. Adachi *et al.* (ILC International Development Team Collaboration), arXiv:2203.07622.
[101] A. Djouadi, Phys. Rep. **459**, 1 (2008).
[102] A. Arbey, M. Battaglia, A. Djouadi, F. Mahmoudi, M. Muhlleitner, and M. Spira, Phys. Rev. D **106**, 055002 (2022).
[103] H. Eberl, K. Hidaka, and E. Ginina (to be published).